Supporting Information for:

Carbon disulfide binding at dinuclear and mononuclear nickel complexes ligated by a redox-active ligand: Iminopyridine serving as an accumulator of redox equivalents for the activation of heteroallenes

Amarnath Bhemaraju, Jeffrey W. Beattie, Richard L. Lord, Philip D. Martin, and Stanislav Groysman*

Department of Chemistry, Wayne State University, Detroit, Michigan 48202, United States.

Index *Page*

1. General methods and procedures

All reactions involving air-sensitive materials were executed in a nitrogen-filled glovebox. p-Xylylenediamine, benzylamine, 2-carboxaldehydepyridine, bis(cyclooctadiene)nickel(0) ($Ni(COD)_2$), carbon disulfide, and ^{13}C-labeled carbon disulfide were purchased from Aldrich, Strem or TCI America and used as received. All solvents were purchased from Fisher scientific and were of HPLC grade. The solvents were purified using an MBRAUN solvent purification system and stored over 3-Å molecular sieves. Compounds were routinely characterized by ^1H and ^{13}C {H} NMR (^{13}C NMR thereafter), X-ray crystallography, and elemental analyses. Selected compounds were characterized by mass spectrometry (ESI). NMR spectra of all compounds were recorded at the Lumigen Instrument Center (Wayne State University) on a Varian Mercury 400 NMR Spectrometer in C_6D_6 or $(CD_3)_2SO$ at room temperature. Chemical shifts and coupling constants (*J*) were reported in parts per million (δ) and Hertz respectively. Low resolution mass spectra were obtained at the Lumigen Instrument Center utilizing a Waters Micromass ZQ mass spectrometer (direct injection, with capillary at 3.573 (KV) and cone voltage of 20.000 (V)). Elemental analyses were performed by Midwest Microlab LLC.

2. Synthesis and characterization of compounds

Preparation of L^1, $Ni_2(L^1)(COD)_2$ (1), $Ni_2L^1(CS_2)_2$ (2), $Ni(L^2)(COD)$ (3), and $Ni(L^2)(CS_2)$ (4).

The synthesis of $\mathbf{L^1}$ and $\mathbf{Ni_2(L^1)(COD)_2}$ has been reported by us previously[1,1], and $\mathbf{L^2}$ was synthesized according to the previously published procedure.[2]

$Ni(L^2)(COD)$ (3). A solution of L^2 (53 mg, 0.27 mmol) in 5 mL of THF was added dropwise at room temperature to a 5 mL solution of bis(cyclooctadiene)nickel(0) ($Ni(COD)_2$) (103 mg, 0.374 mmol) in THF. The resulting violet-blue colored reaction mixture was stirred for 1 h, and the solvent was removed in *vacuo*. Crystallization from hexanes resulted in violet-blue crystalline solid (70 mg, 71 %). ^1H NMR (C_6D_6, 400 MHz) δ 10.10 (d, *J = 6.8*, 1H), 8.23 (s, 1H), 7.31-7.27 (m, 2H), 7.23-7.18 (m, 2H), 7.17-7.10 (m, 2H), 7.07 (m, 1H), 6.92 (dt, *J = 8.0, 1.2*, 1H), 5.29 (s, *2*H), 3.77 (m, *2*H), 3.70 (m, *2*H), 2.74 (m, 2H), 2.51 (m, *2*H), 1.74-1.57 (m, 4H); ^{13}C NMR (C_6D_6, 75 MHz) δ 152.22, 147.96, 142.60, 139.86, 128.60, 128.42, 127.63, 127.44, 127.16, 125.47, 118.98, 82.97, 82.06, 66.38, 31.36, 31.32. Anal. Calcd for $C_{21}H_{24}N_2Ni \cdot C_4H_{10}O$: C, 68.67; H, 7.84; N, 6.41. Found: C, 68.19; H, 6.65; N, 6.03.

$NiL^2(CS_2)$ (4). A 0.083 M solution of CS_2 (1.38 ml, 0.115 mmol) in THF, was added to the 3 mL of violet-blue $Ni(L^2)(COD)$ (60 mg, 0.165 mmol) solution in diethyl ether. A precipitate was obtained after the addition of the CS_2 solution. An additional 4 mL of diethyl ether was added to the reaction mixture and it was stirred for 10 minutes. Crystallization of the insoluble precipitate using CH_3CN and ether resulted in a crystalline purple-brown solid (32 mg, 84 %). ^1H NMR (DMSO-d6, 400 MHz) δ 9.47 (d, *J = 4.8*, 1H), 8.93 (s, 1H), 8.22 (t, *J = 7.6*, 1H), 7.98 (d, *J = 7.6*, 1H), 7.91 (t, *J = 6.4*, 1H), 7.48 (d, *J = 7.2*, 2H), 7.41-7.27 (m, 3H), 5.23 (m, *2*H); ^{13}C NMR (DMSO-d6, 75 MHz) δ 267.90 ($^{13}CS_2$), 165.75, 152.50, 148.36, 138.63, 136.36, 130.76, 128.48, 128.33, 128.12, 128.05, 127.27, 126.33, 62.10. MS (ESI) calcd for $[Ni(L^2)]^+$ 254.03, found 253.11. We were not able to observe the parent ion in the mass spectrum. The compound is unstable, decomposing over time as demonstrated below. The attempted EA shows low carbon

percentage. Anal. Calcd for $C_{14}H_{12}N_2NiS_2$: C, 50.79; H, 3.65; N, 8.46. Found: C, 46.34; H, 3.52; N, 7.24.

Reaction of $Ni_2L^1(^{13}CS_2)_2$ with unlabelled CS_2. A solution of 5 mg of **$Ni_2L^1(^{13}CS_2)$** in DMSO-d_6 was treated with ca. 3 equiv of CS_2. ^{13}C NMR spectrum (600 scans, Figure S12) was collected has demonstrated no signals attributable to $^{13}CS2$. The solution was left overnight at RT, and another ^{13}C NMR spectrum (600 scans, Figure S13) was collected. The peak at 193 ppm (free $^{13}CS_2$) was observed.

Reaction of $Ni_2L^1(^{13}CS_2)_2$ with $[FeCp_2](PF_6)$. A deep-purple solution of 22 mg of **$Ni_2L^1(^{13}CS_2)$** in 2 mL of DMSO-d_6 was treated with 2 equiv (25 mg) of $[FeCp_2](PF_6)$. An immediate color change to yellow was observed, and was followed by a slow color change to purple. ^1H NMR (Figure S14) displayed a peak at 4.16 ppm ($FeCp_2$). In addition, small amount of the unreacted starting material ($Ni_2L^1(^{13}CS_2)_2$) was also observed. ^{13}C NMR spectrum (1200 scans, Figure S15) has displayed a signal at 192 ppm (free $^{13}CS_2$) and 67 ppm ($FeCp_2$). Addition of another batch of $[FeCp_2](PF_6)$ (18 mg) resulted in a yellow-green solution. ^1H NMR of this solution contained no peaks attributed to $(Ni_2L^1(^{13}CS_2)_2$; a very broad resonance (that we attribute to the mixture of $FeCp_2$/$[FeCp_2](PF_6)$) was observed around 6.2 ppm (Figure S16). ^{13}C NMR (Figure S17) demonstrated significantly larger resonance (versus internal standard – toluene) at 192 ppm (free $^{13}CS_2$) compared to ^{13}C NMR of the reaction of **$Ni_2L^1(^{13}CS_2)$** with 2 equiv of $[FeCp_2](PF_6)$ (See Figure S15).

Reaction of $Ni_2L^1(CS_2)_2$ with PPh_3. A solution of 12 mg of **$Ni_2L^2(CS_2)$** in DMSO-d_6 was treated with 2 equiv of PPh_3 (11 mg, 0.042 mmol). No color change was observed. The solution was stirred overnight at RT. ^1H and ^{31}P NMR spectra demonstrated only starting materials present (See Figure S18 for ^1H NMR and Figure S19 for ^{31}P NMR).

3. X-ray crystallographic details

Structures of **2-4** were confirmed by X-ray analysis. The crystals were mounted on a Bruker APEXII/Kappa three circle goniometer platform diffractometer equipped with an APEX-2 detector. A graphic monochromator was employed for wavelength selection of the Mo Kα radiation (λ = 0.71073 Å). The data were processed and refined using the program SAINT supplied by Siemens Industrial Automation. Structures were solved by direct methods in SHELXS and refined by standard difference Fourier techniques in the SHELXTL program suite (6.10 v., Sheldrick G. M., and Siemens Industrial Automation, 2000). Hydrogen atoms were placed in calculated positions using the standard riding model and refined isotropically; all other atoms were refined anisotropically. In the structure of 2, $Ni_2L^1(CS_2)_2$ occupies a special position. The structure of **4** contained two crystalographically independent molecules of $L^2Ni(CS_2)$, displaying slightly different metrics (Figure S1).

4. X-ray structure of 4

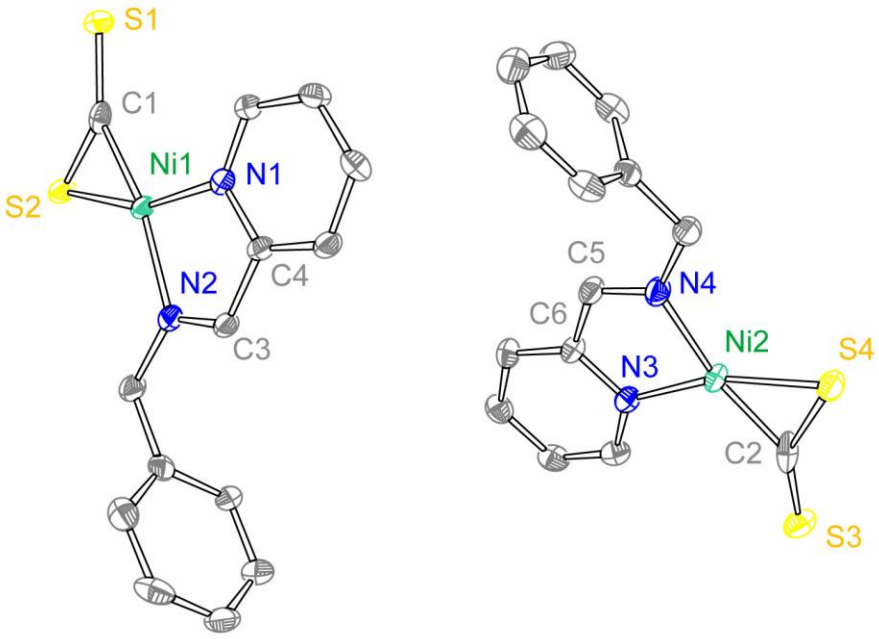

Figure S1. X-ray structure of **4**, 50% probability ellipsoids. Selected bond distances: S1 C1 1.548(8) Å, S2 C1 1.745(8) Å, S3 C2 1.617(7) Å, S4 C2 1.686(7) Å, N2 C3 1.271(7) Å, C3 C4 1.454(7) Å, N4 C5 1.267(7) Å, C5 C6 1.468(7) Å.

5. ^{1}H, ^{13}C and ^{31}P-NMR Spectra

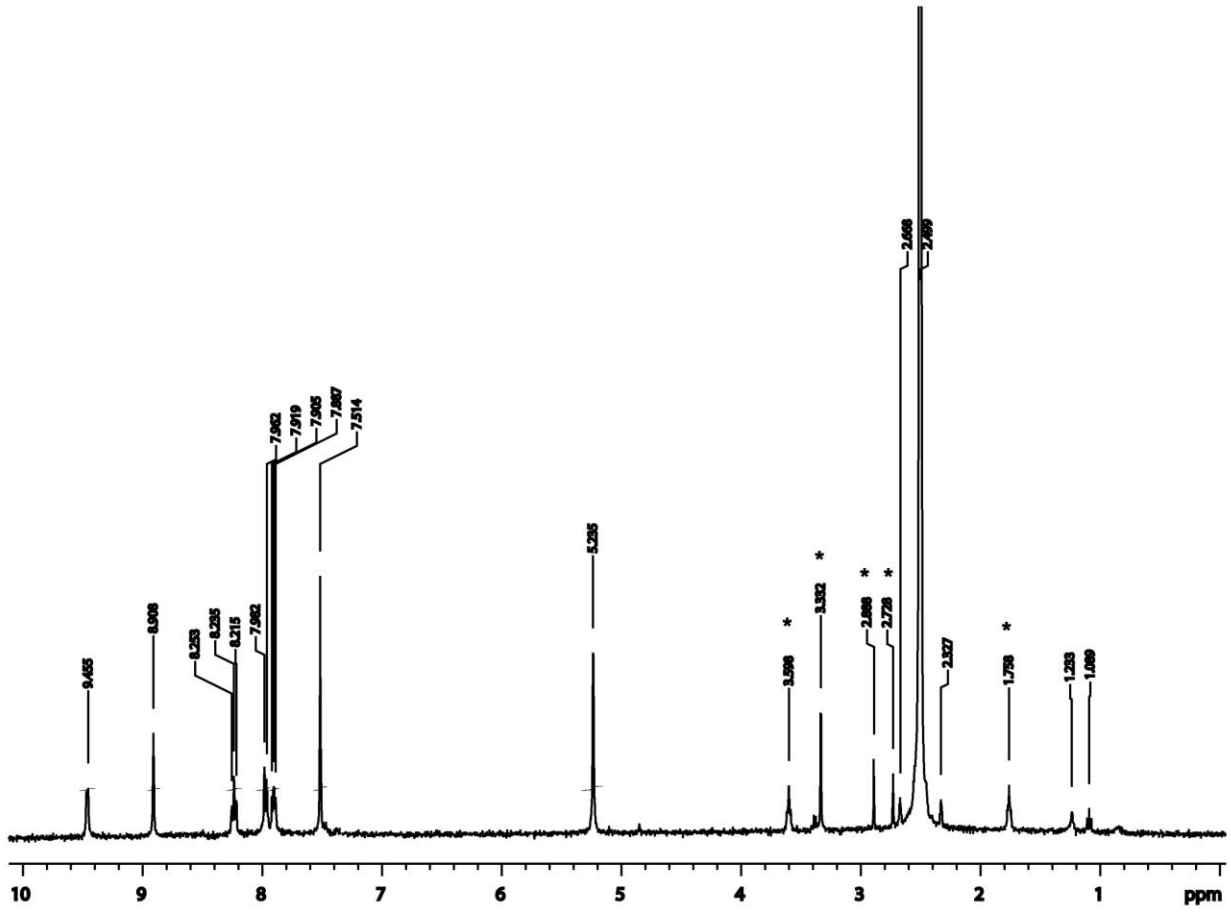

Figure S2. ^{1}H NMR of $Ni_2(L^1)(CS_2)_2$ (**2**). Solvent peaks (indicated by ∗): 3.598: THF; 3.332: H_2O; 1.759: THF; 2.888: DMF; 2.728: DMF.

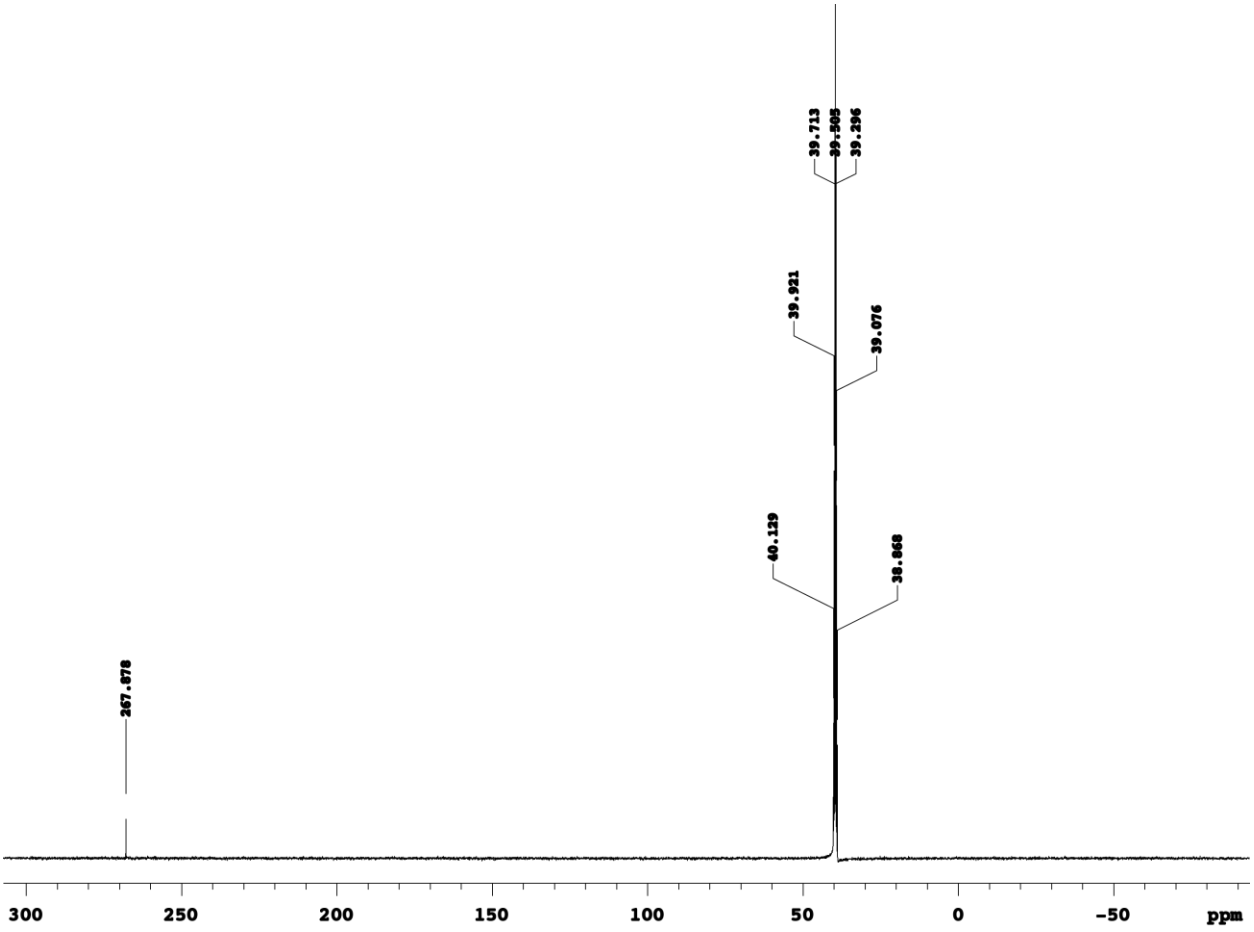

Figure S3. ^{13}C NMR of $Ni_2(L^1)(^{13}CS_2)_2$ (**2**-$^{13}CS_2$).

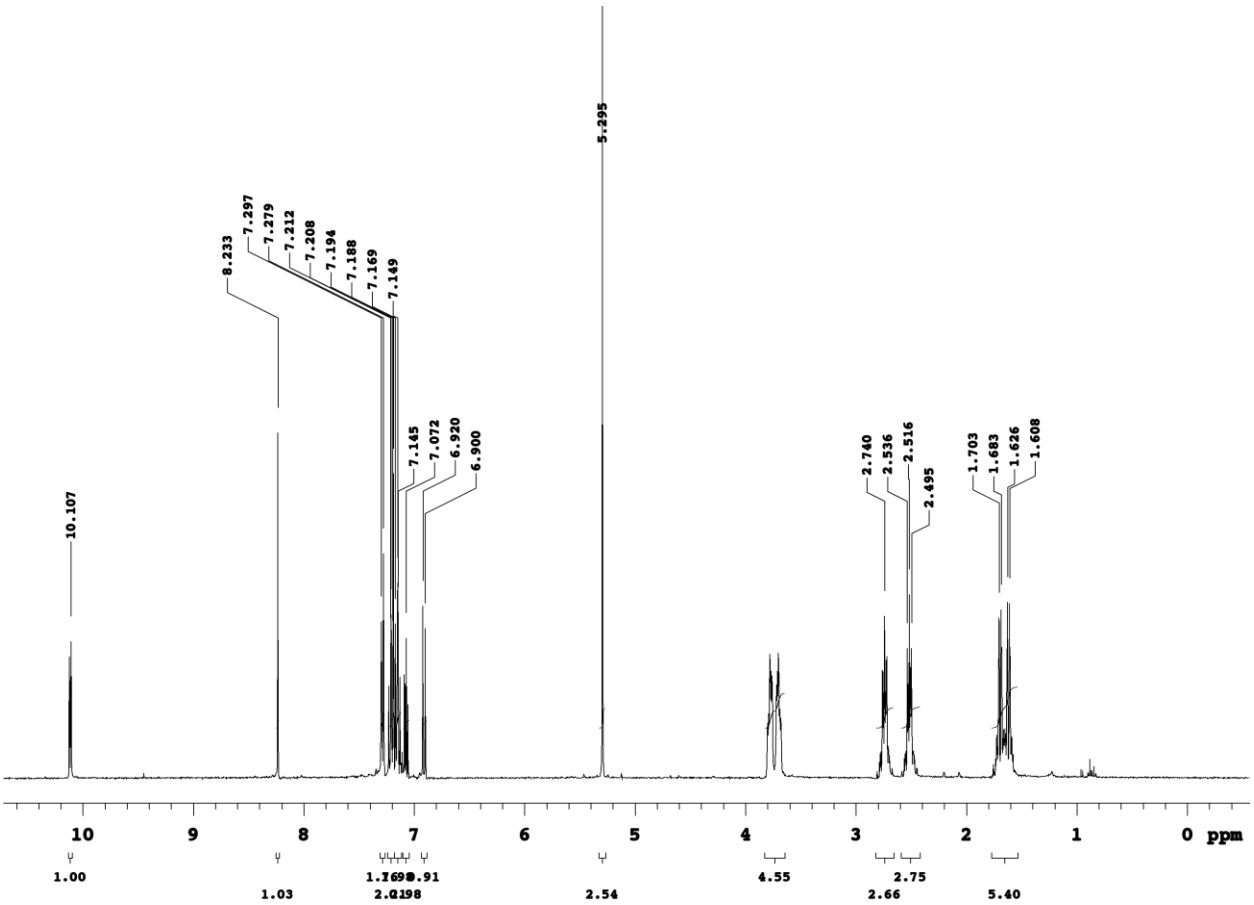

Figure S4. ^{1}H NMR of Ni(L^{2})(COD) (**3**).

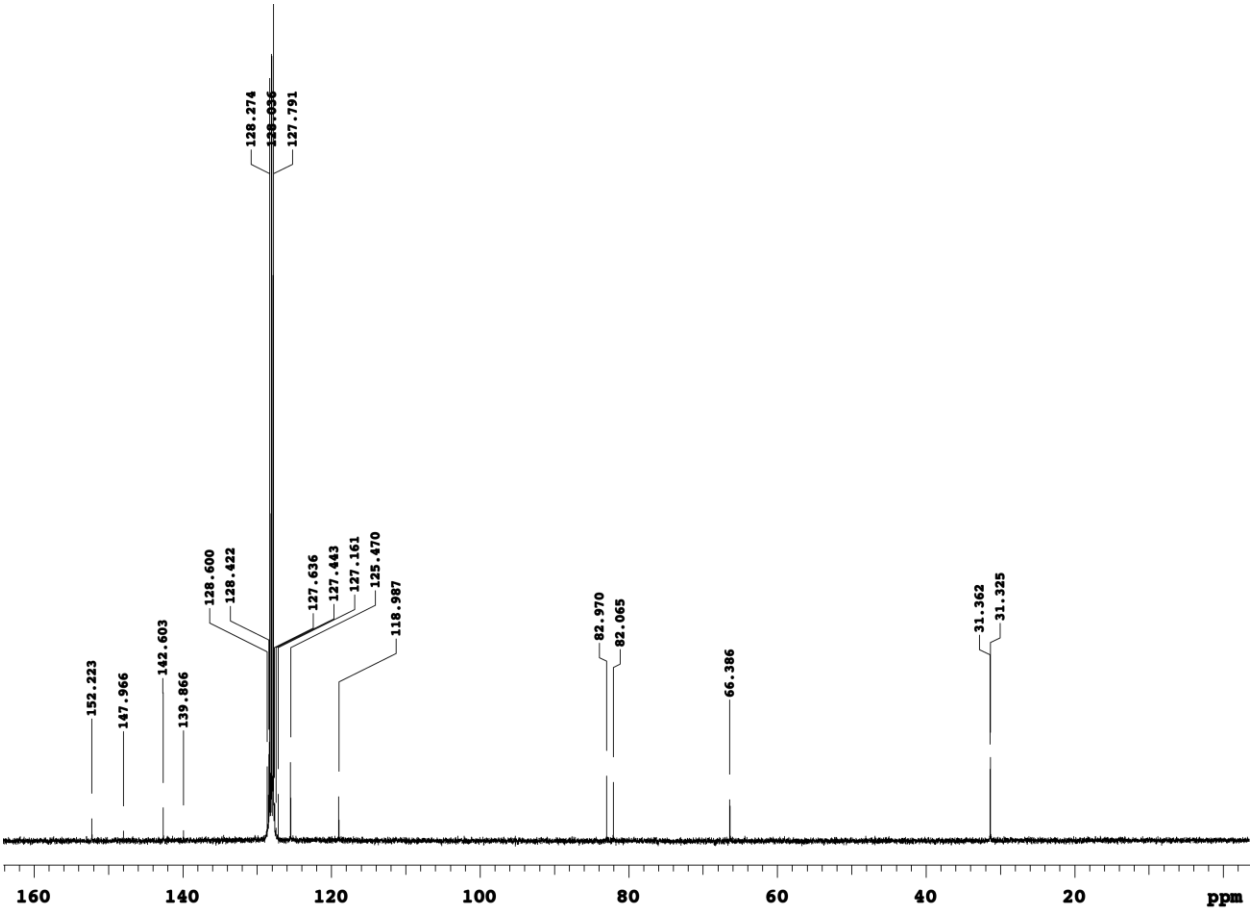

Figure S5. ^{13}C NMR of Ni(L^2)(COD) (**3**).

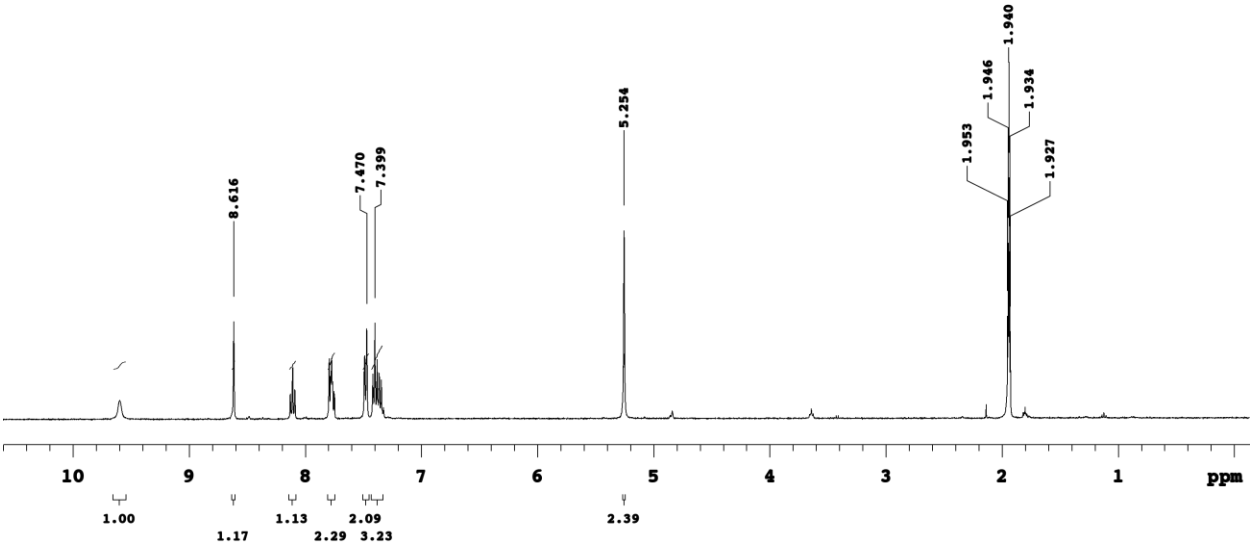

Figure S6. ^{1}H NMR of Ni(L^{2})(CS_2) (**4**) in CD_3CN.

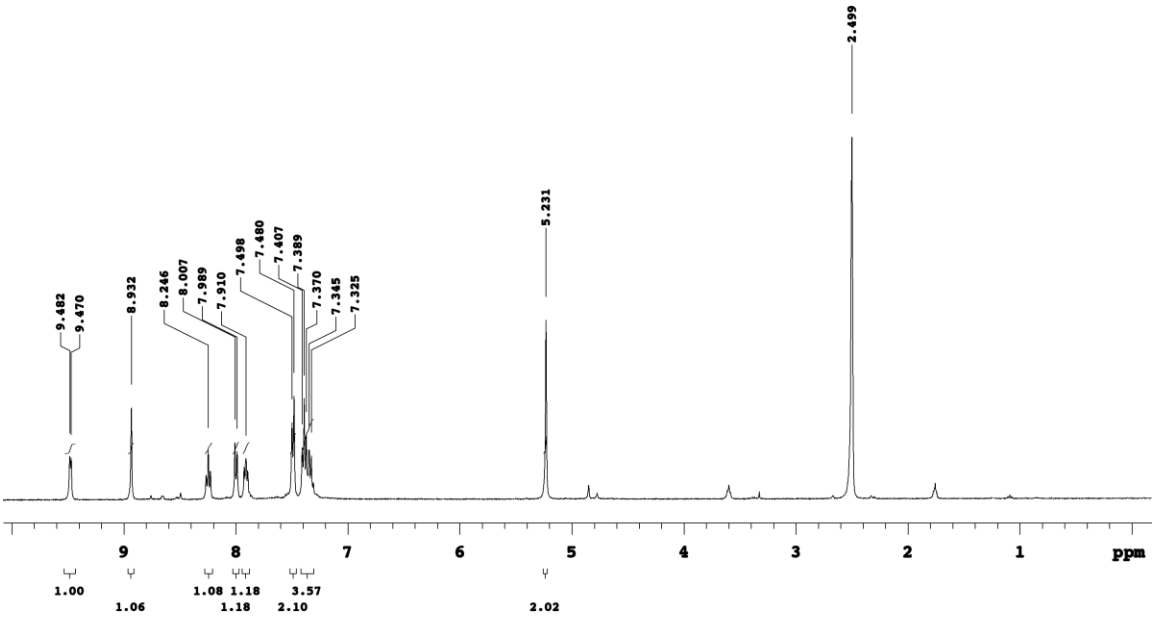

Figure S7. ^{1}H NMR of **4** in DMSO.

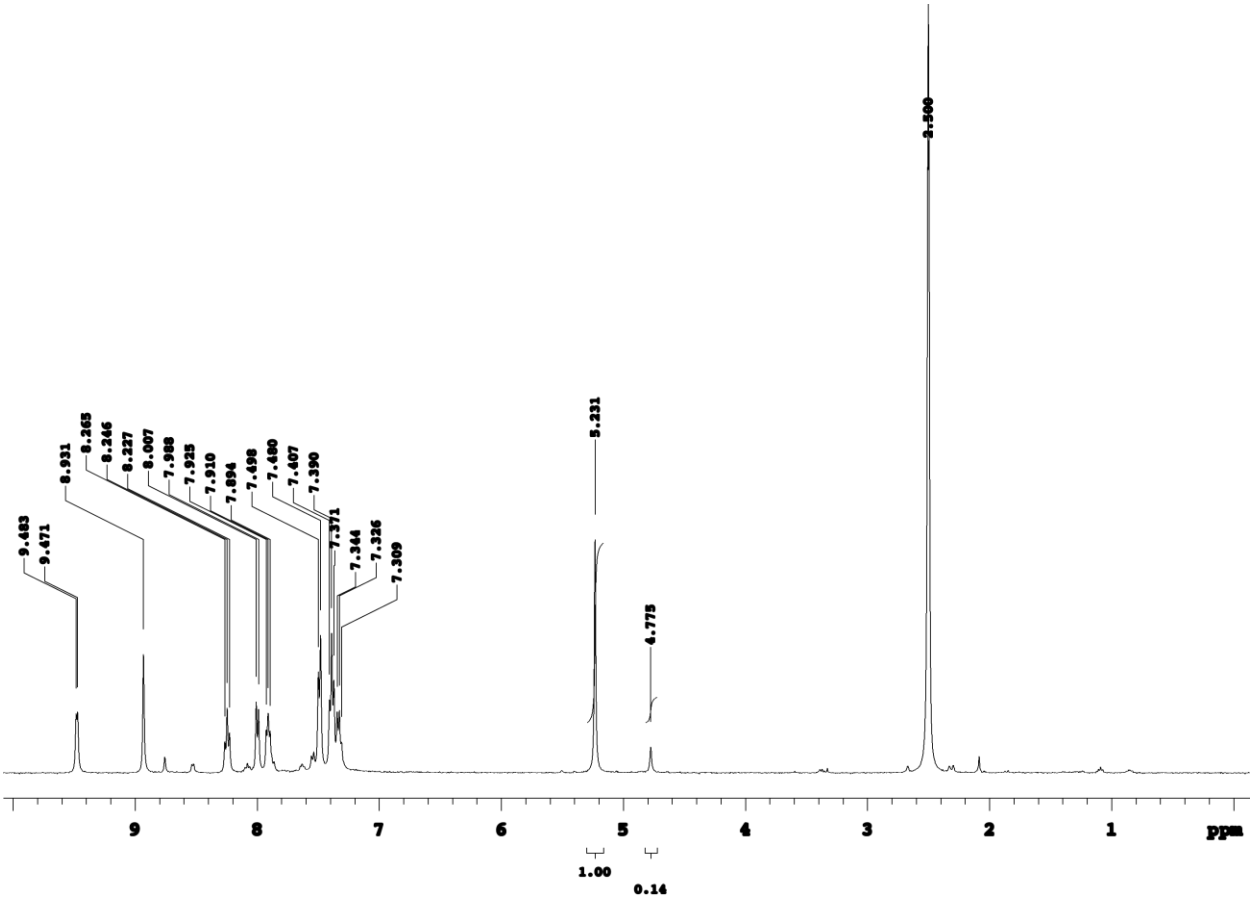

Figure S8. ^{1}H NMR of **4** after 10 min at RT (in DMSO). Ratio between peaks at 5.331 and 4.775 (decomposition product) is 1 : 0.14.

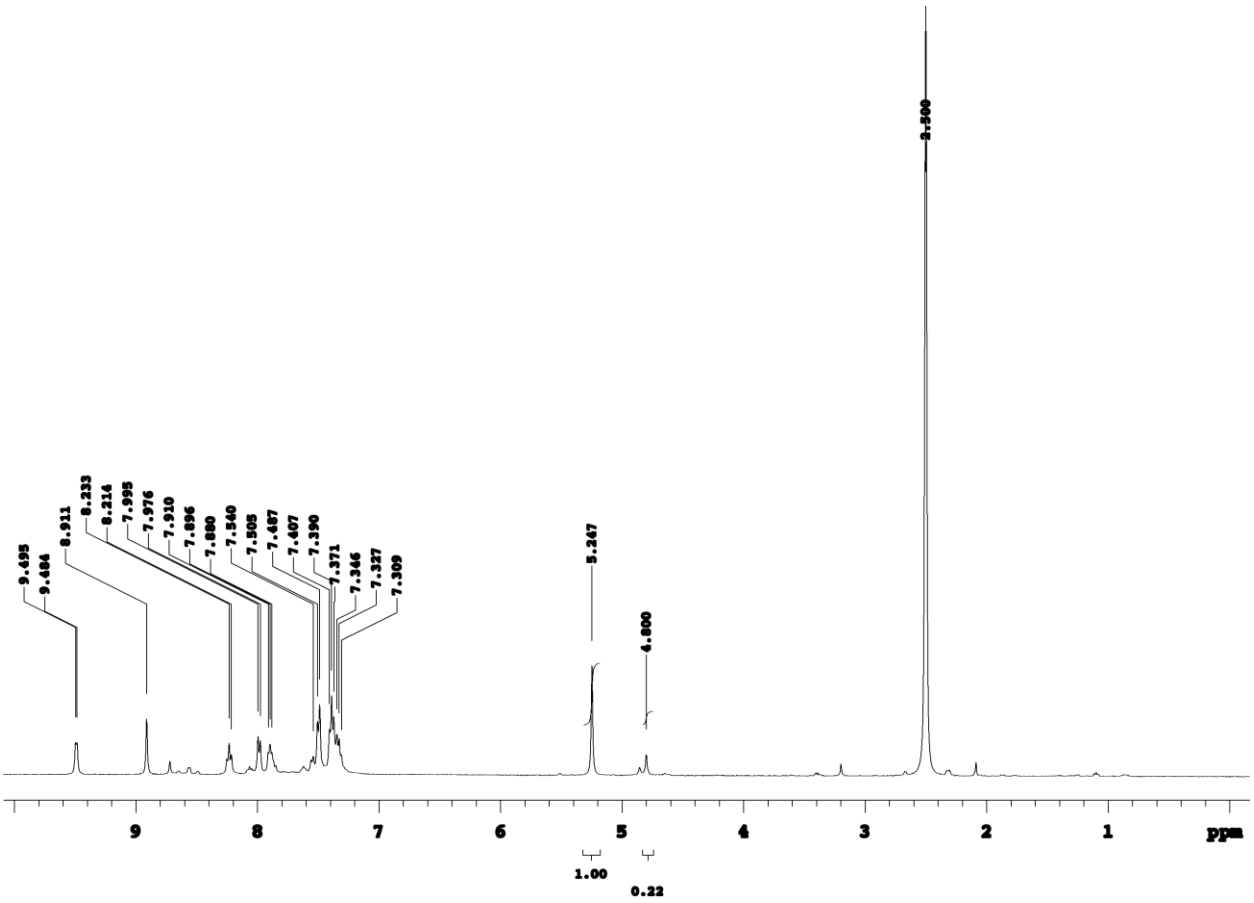

Figure S9. ^{1}H NMR of **4** after 60 min at 50 ^{o}C. Ratio between peaks at 5.247 and 4.800 (decomposition product) is 1 : 0.22.

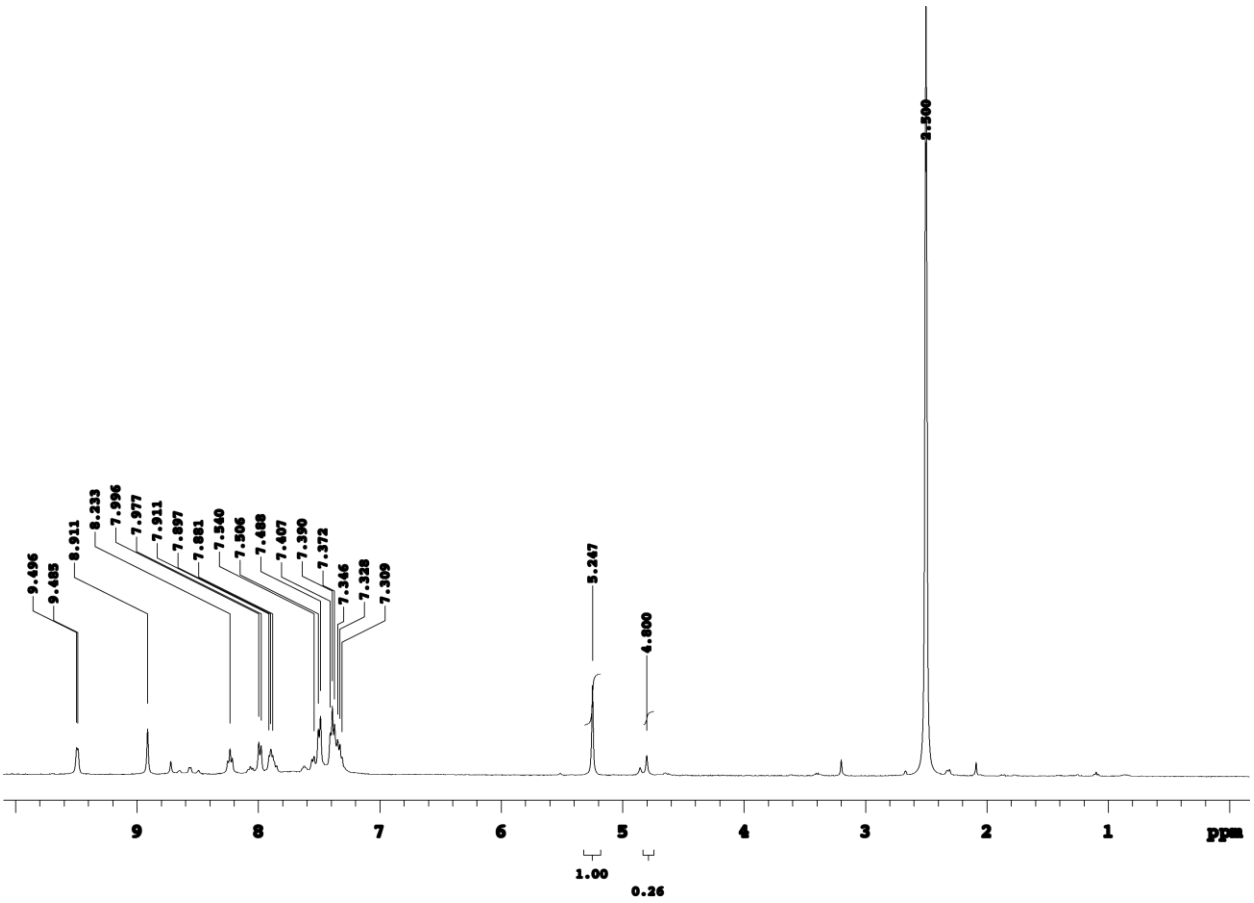

Figure S10. ^{1}H NMR of **4** after 90 min at 50 ^{o}C. Ratio between peaks at 5.247 and 4.800 (decomposition product) is 1 : 0.26.

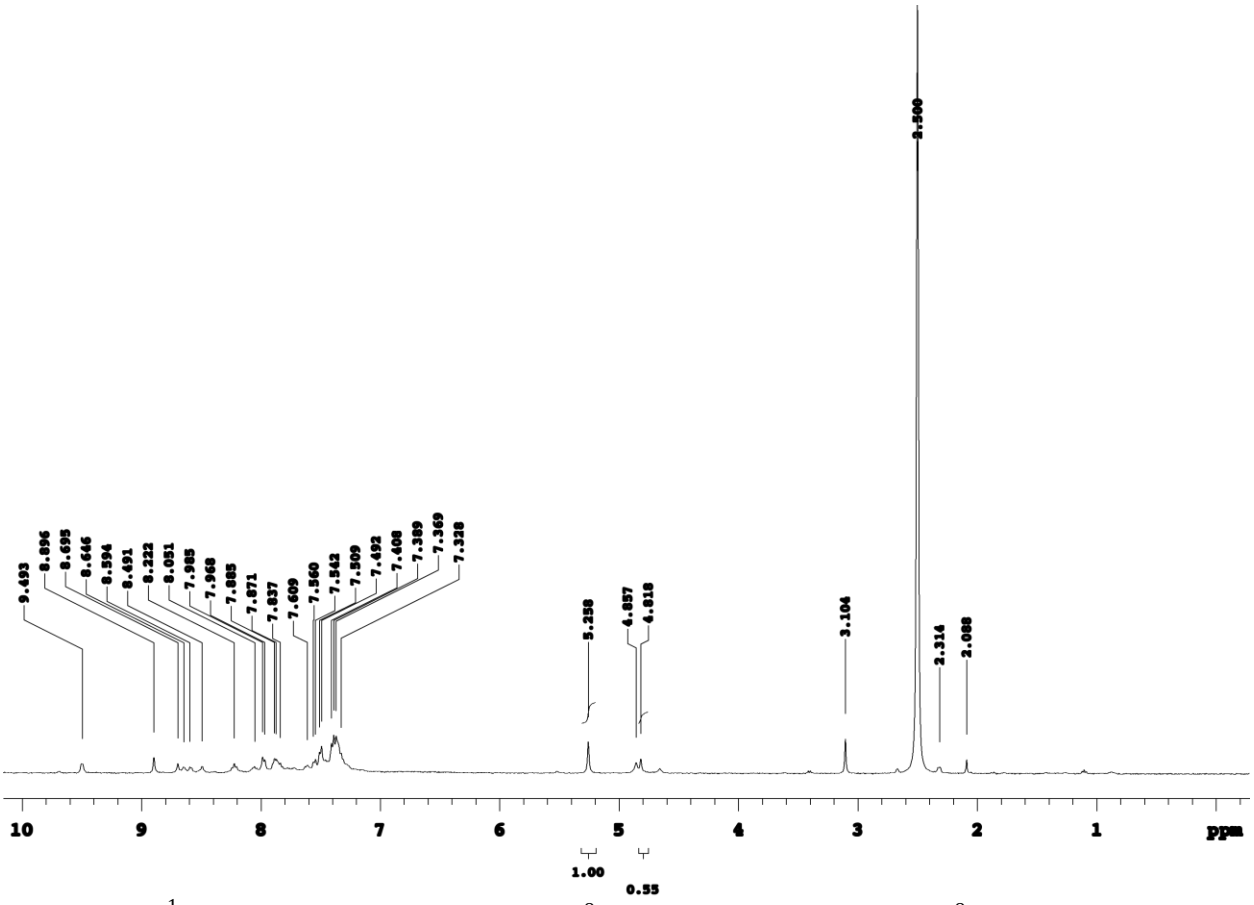

Figure S11. ^{1}H NMR of **4** after 90 min at 50 ^{o}C followed by 60 min at 70 ^{o}C. Ratio between peaks at 5.258 and 4.818 is 1 : 0.55.

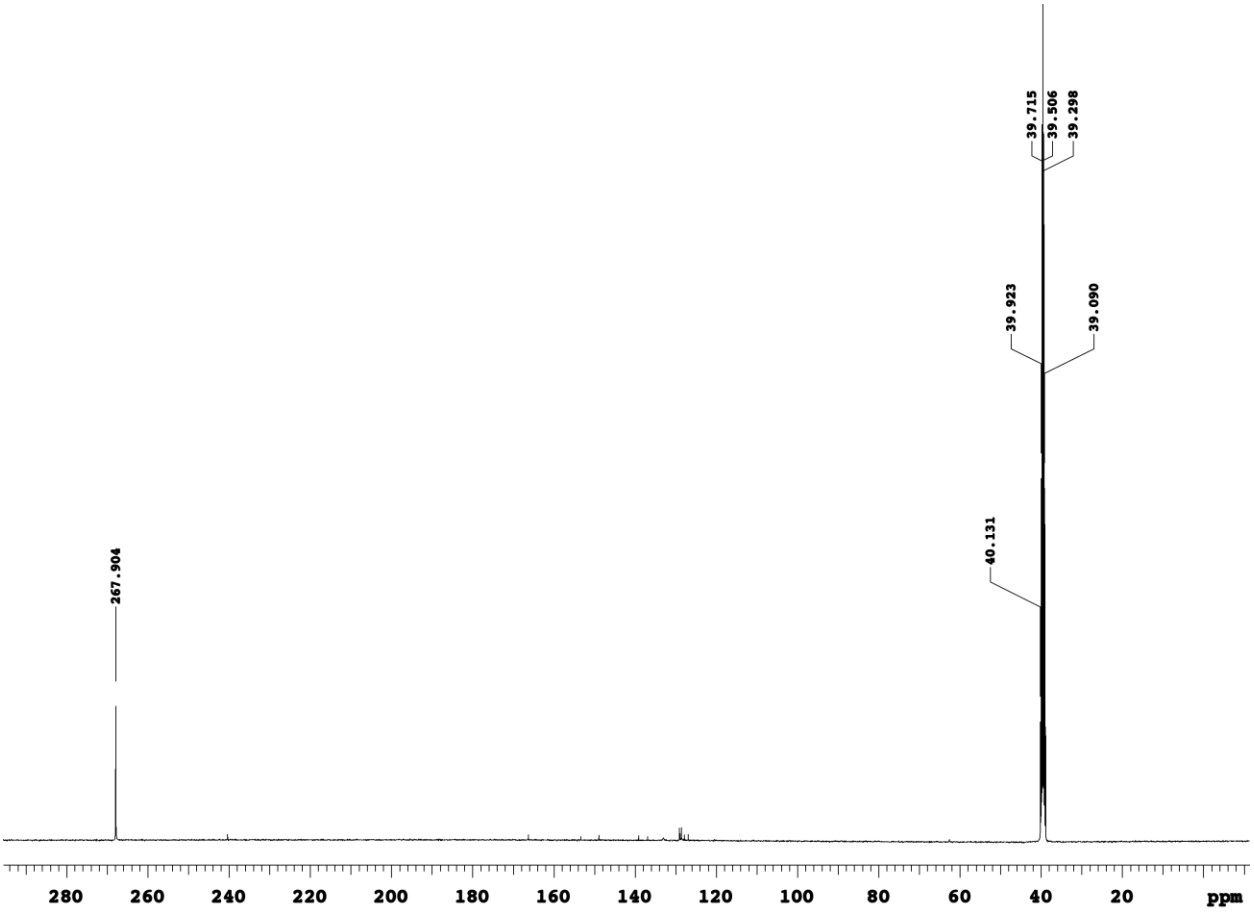

Figure S12. ^{13}C NMR of **4**-$^{13}CS_2$ showing $^{13}CS_2$ signal.

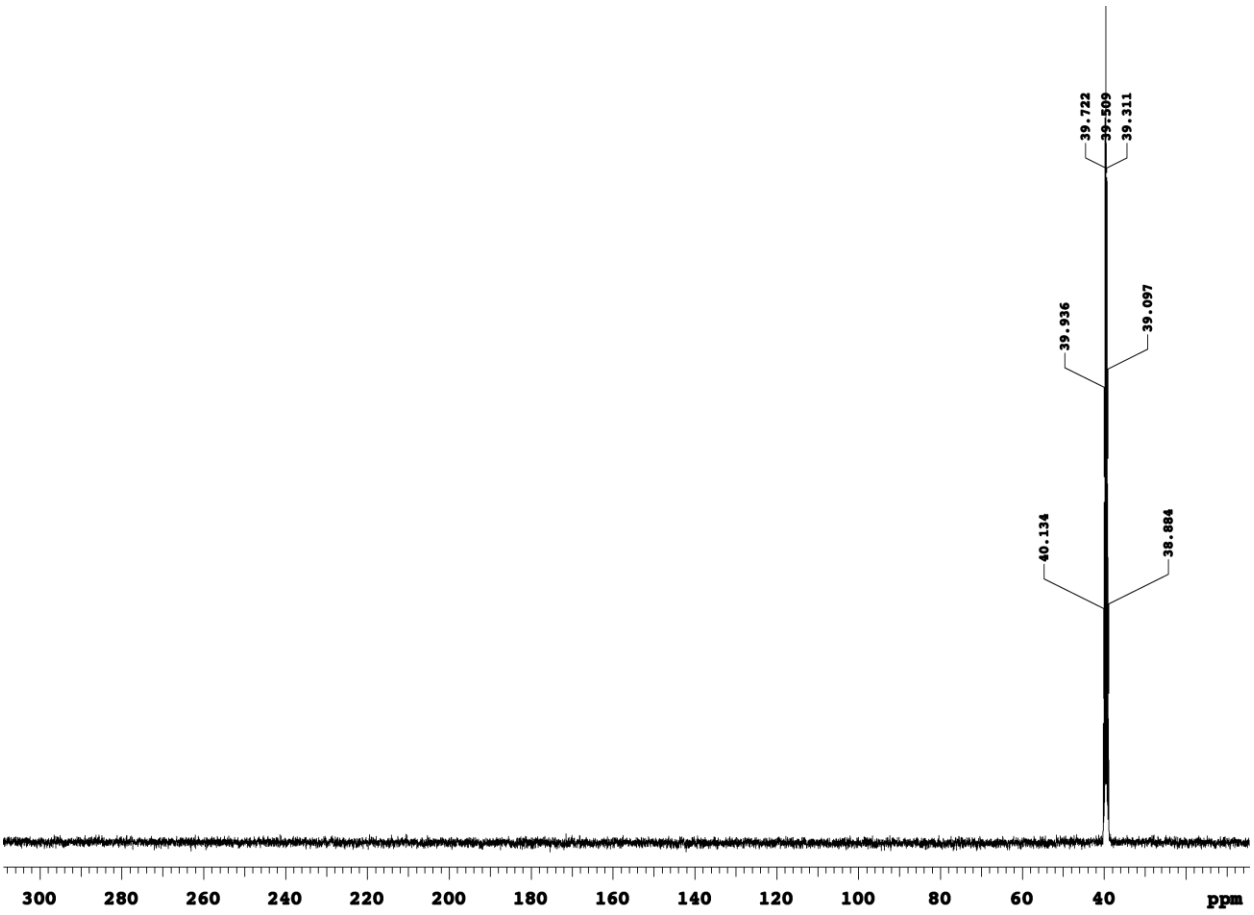

Figure S13. ^{13}C NMR of reaction of $Ni_2L^2(^{13}CS_2)_2$ (**2**-$^{13}CS_2$) with unlabelled CS_2 after 1 h.

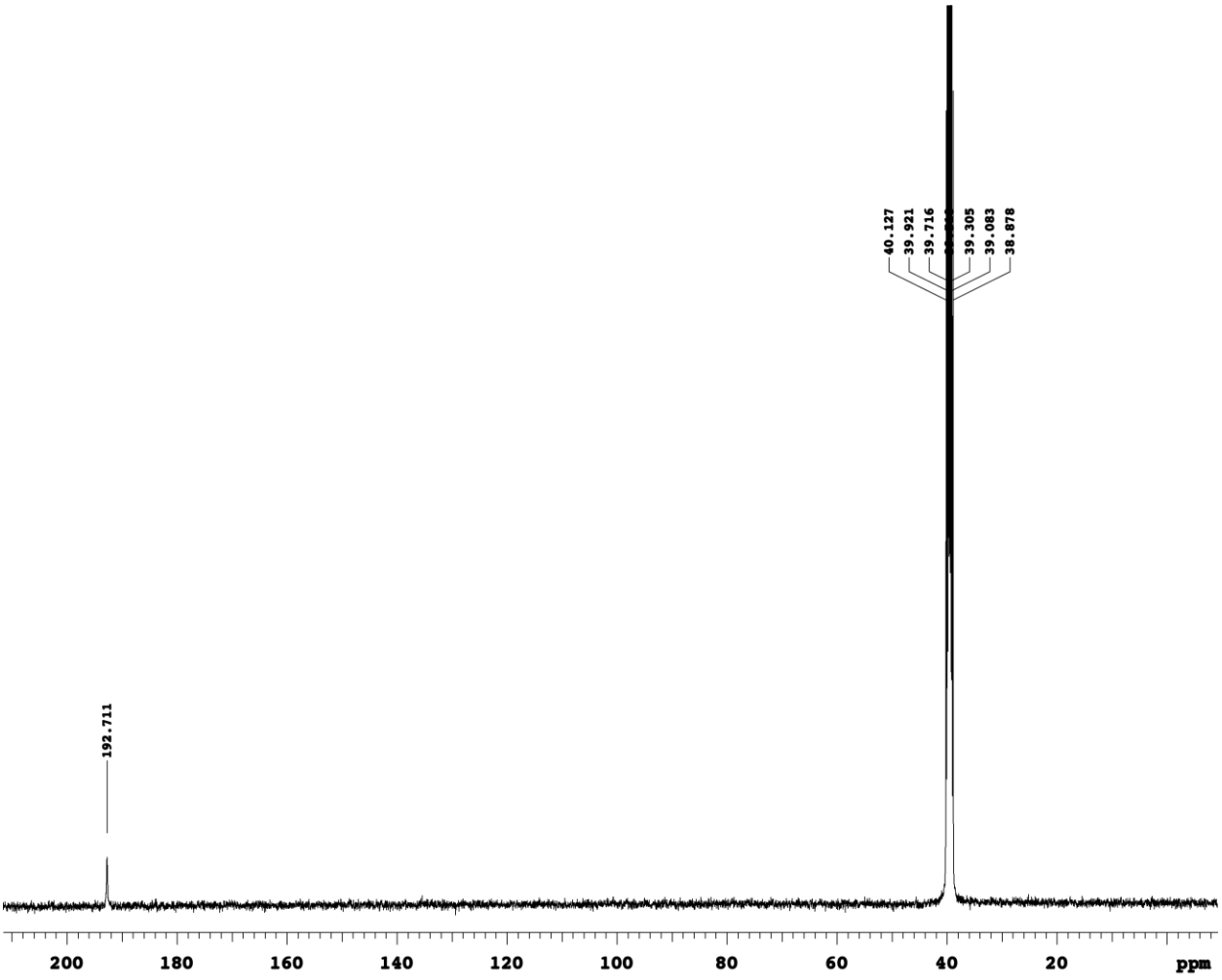

Figure S14. ^{13}C NMR of reaction of $Ni_2L^2(^{13}CS_2)_2$ (**2**-$^{13}CS_2$) with unlabelled CS_2 after 12 h

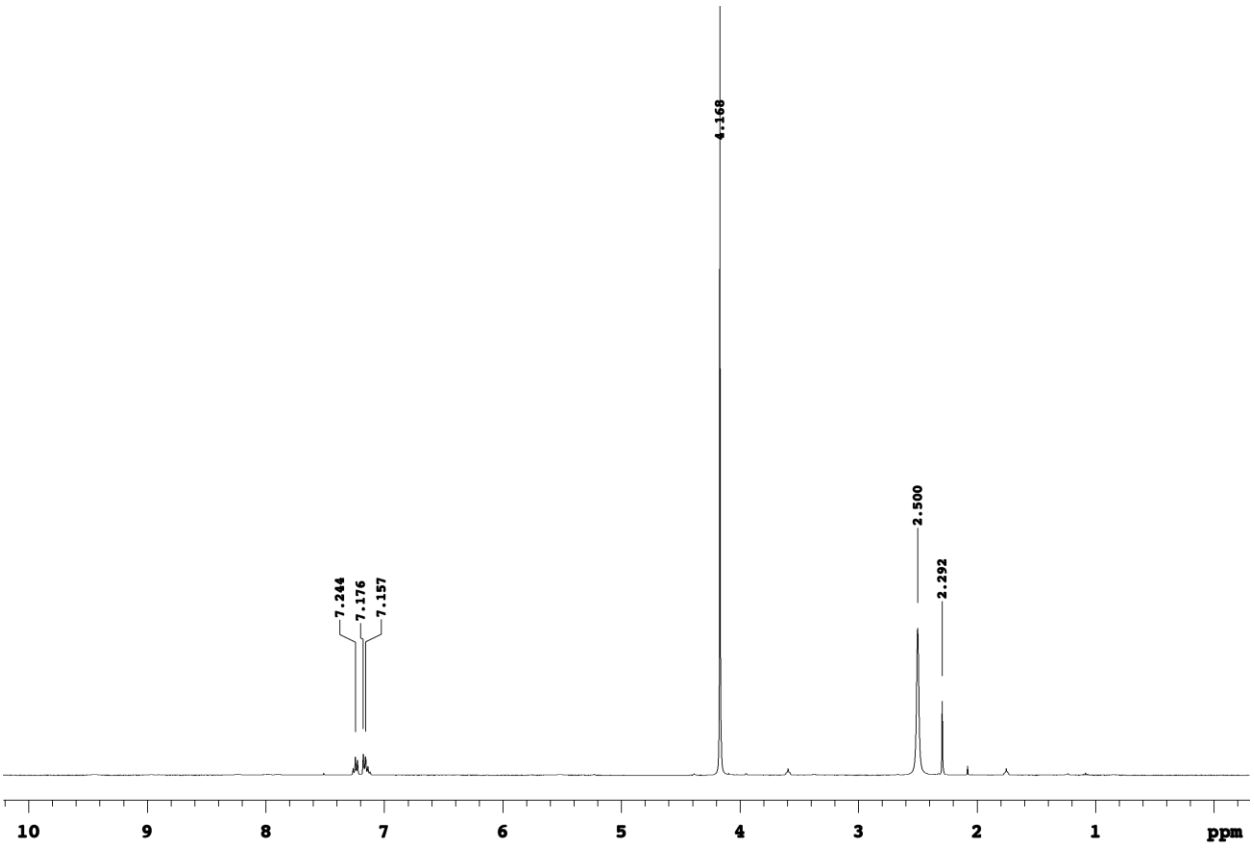

Figure S15. ^{1}H NMR of $Ni_2L^2(^{13}CS_2)_2$ (**2**-$^{13}CS_2$) with 2 equiv of $[FeCp_2](PF_6)$ (the spectrum contains toluene as an internal standard).

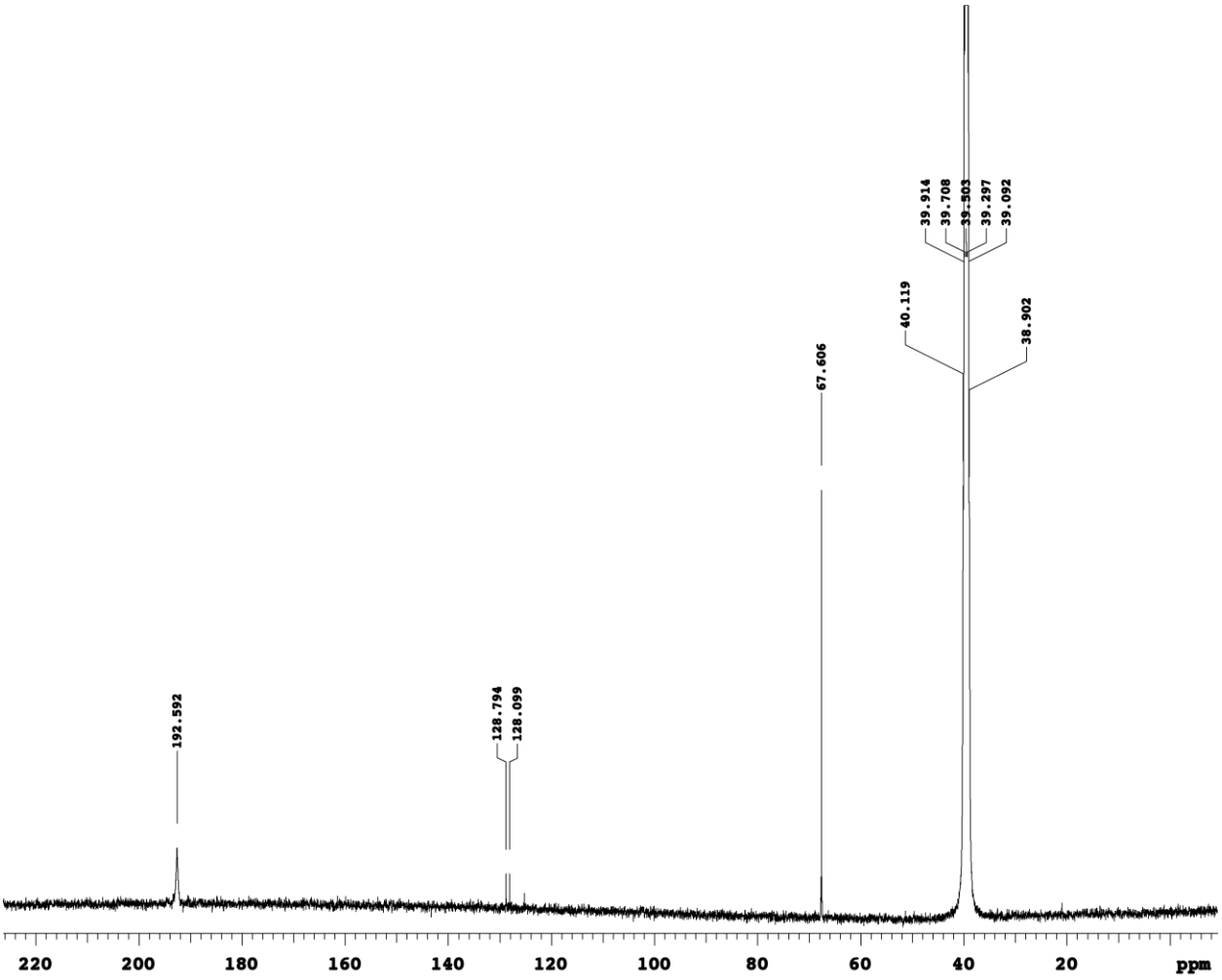

Figure S16. ^{13}C NMR of $Ni_2L^2(^{13}CS_2)_2$ (**2**-$^{13}CS_2$) with 2 equiv. of $[FeCp_2](PF_6)$.

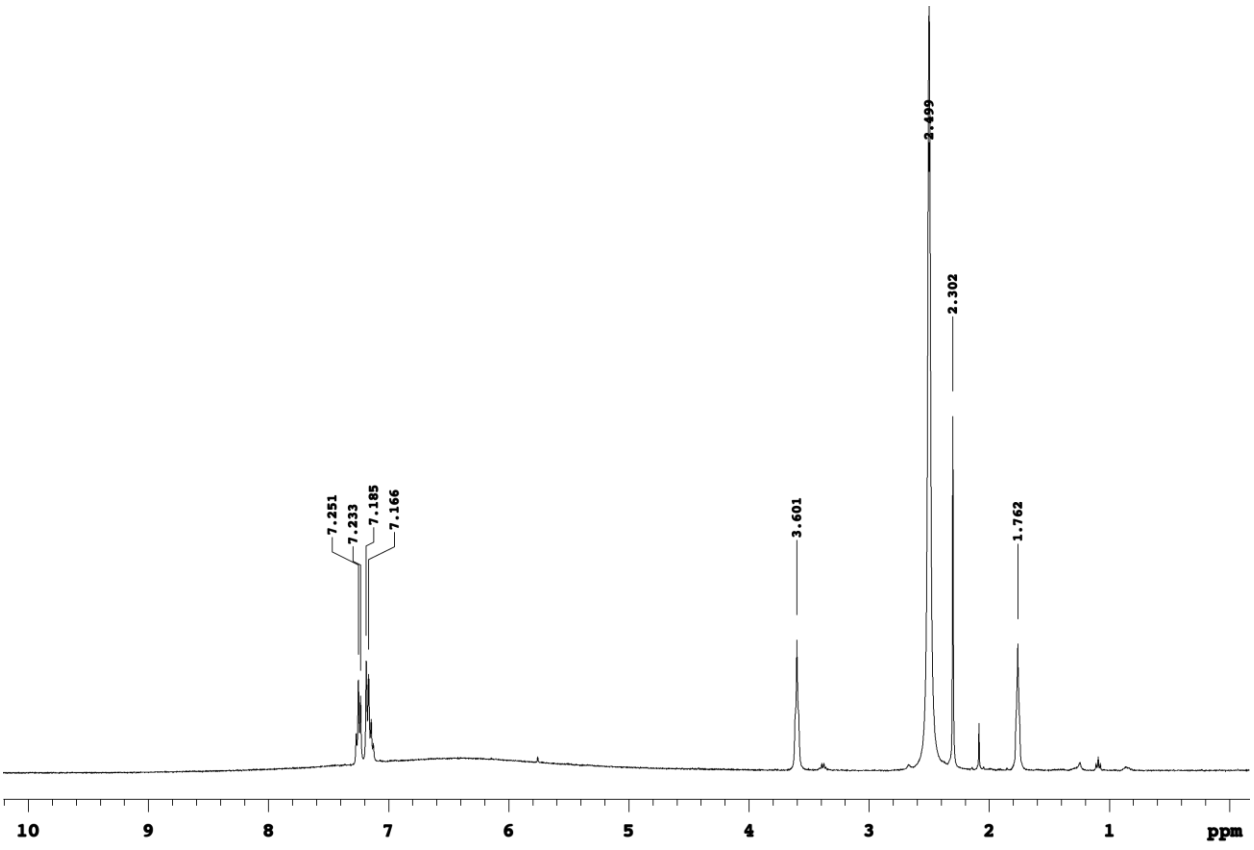

Figure S17. ^{1}H NMR of $Ni_2L^2(^{13}CS_2)_2$ (**2-**$^{13}CS_2$) with 4 equiv of $[FeCp_2](PF_6)$.

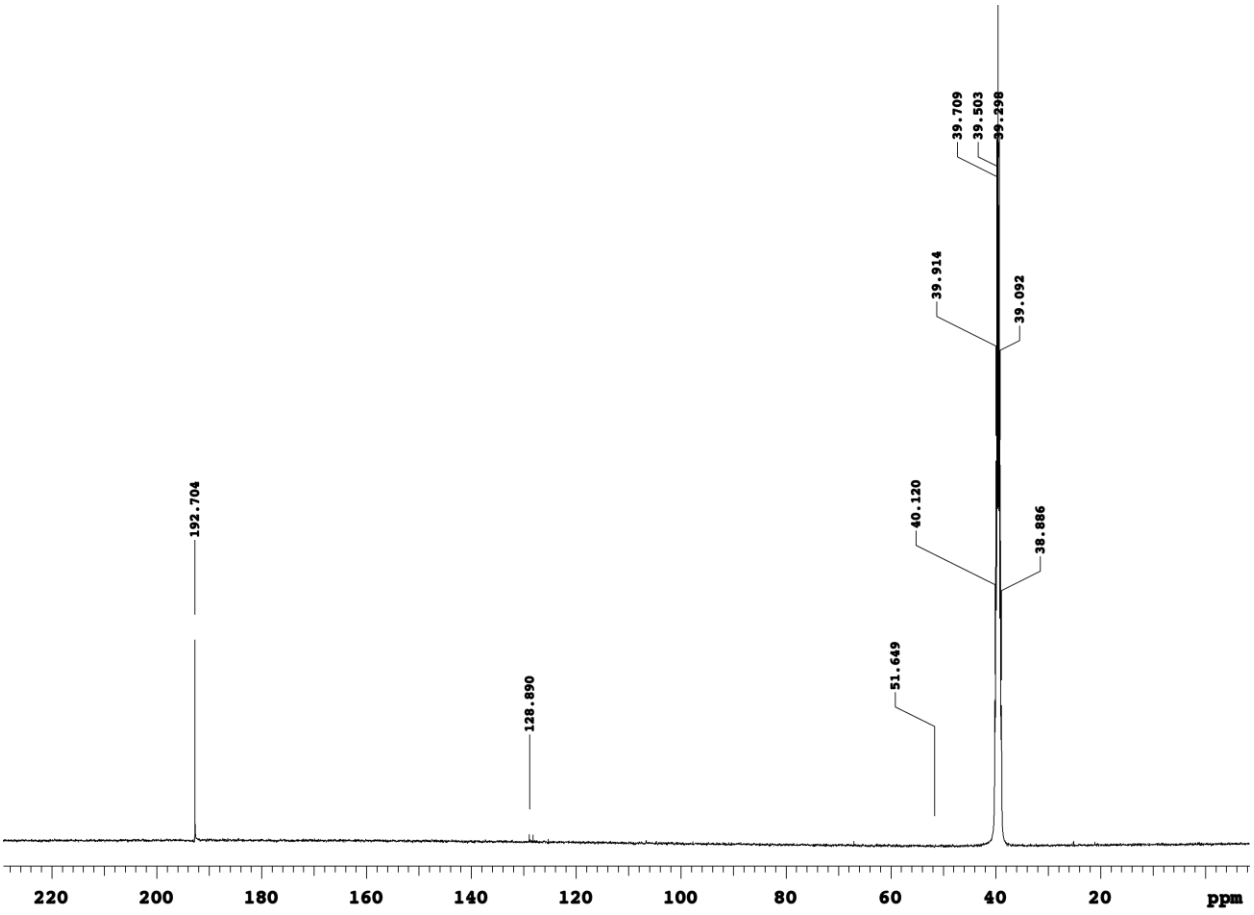

Figure S18. ^{13}C NMR of $Ni_2L^2(^{13}CS_2)_2$ (**2**-$^{13}CS_2$) with 4 equiv of $[FeCp_2](PF_6)$.

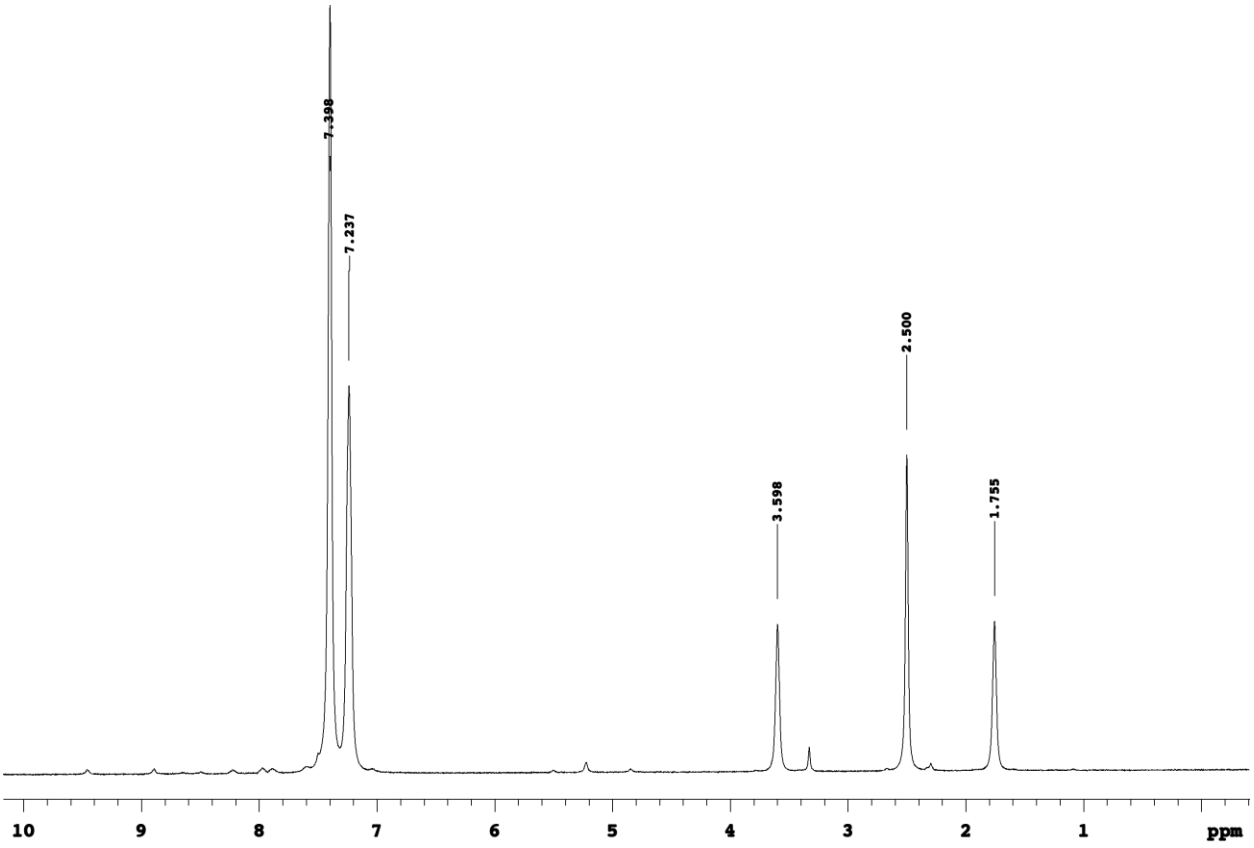

Figure S19. ^{1}H NMR of $Ni_2L^1(CS_2)_2$ (**2**) and PPh_3.

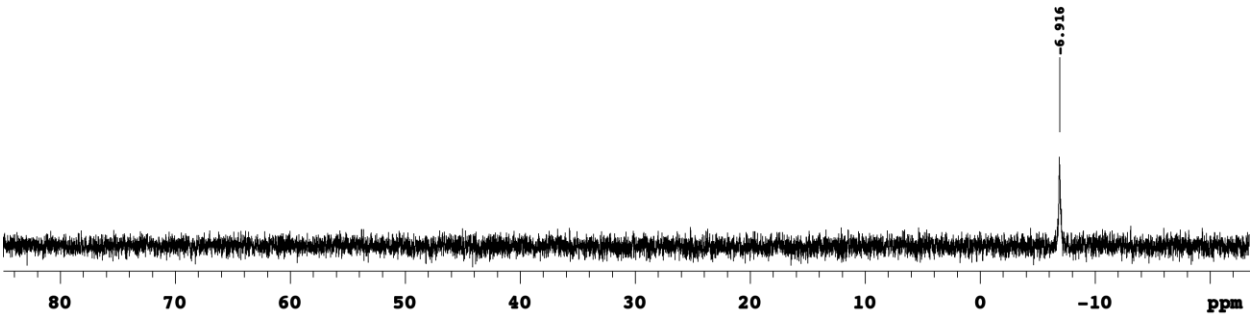

Figure S20. ^{31}P NMR of $Ni_2L^1(CS_2)_2$ (**2**) and PPh_3

6. Mass Spectra

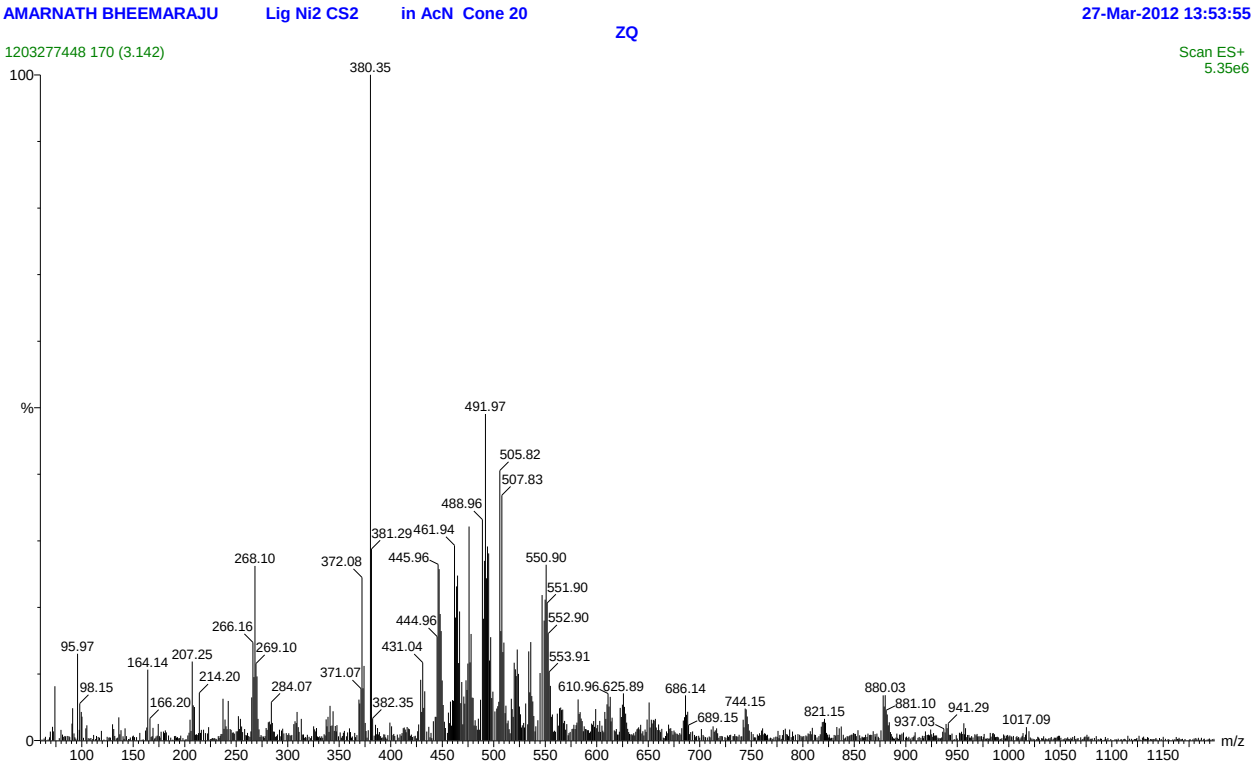

Figure S21. MS of $Ni_2L^1(CS_2)_2$ (**2**).

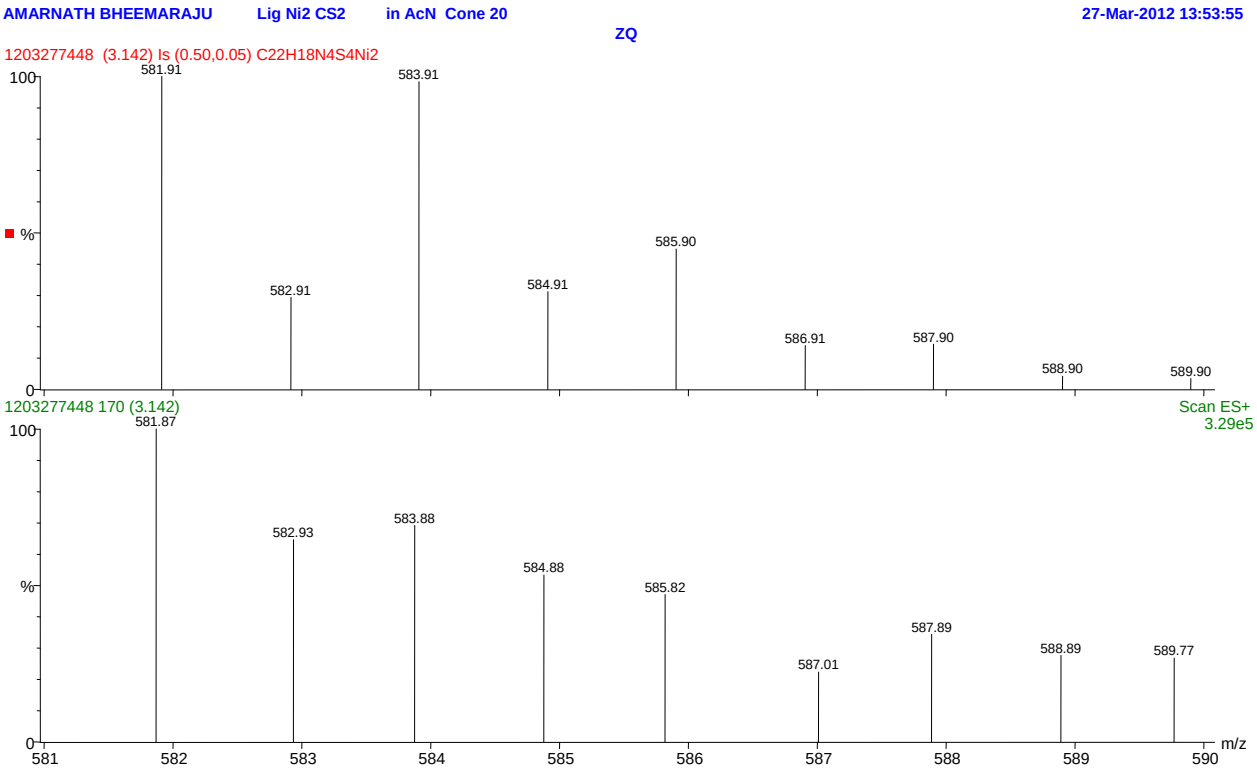

Figure S22. Peak attributed to $[Ni_2L^1(CS_2)_2]^+$ **(2^+)**. Above: calcd for $[Ni_2(L^1)(CS_2)_2]^+$ 581.9. Below: found 581.8.

.

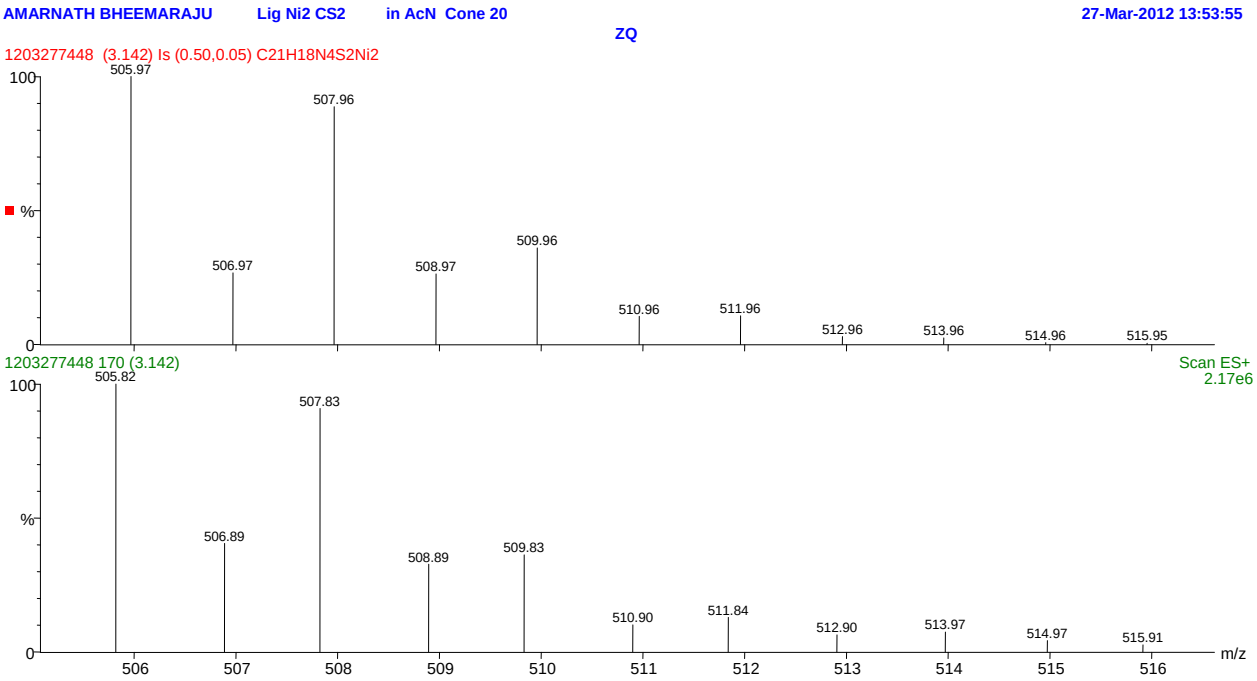

Figure S23. Peak attributed to $[(Ni_2(L^1)CS_2)]+$ ([**2** – CS_2]+) Above: calcd for $[Ni_2(L^1)(CS_2)]^+$ 505.9. Below: found 505.8.

7. FT-IR Spectra

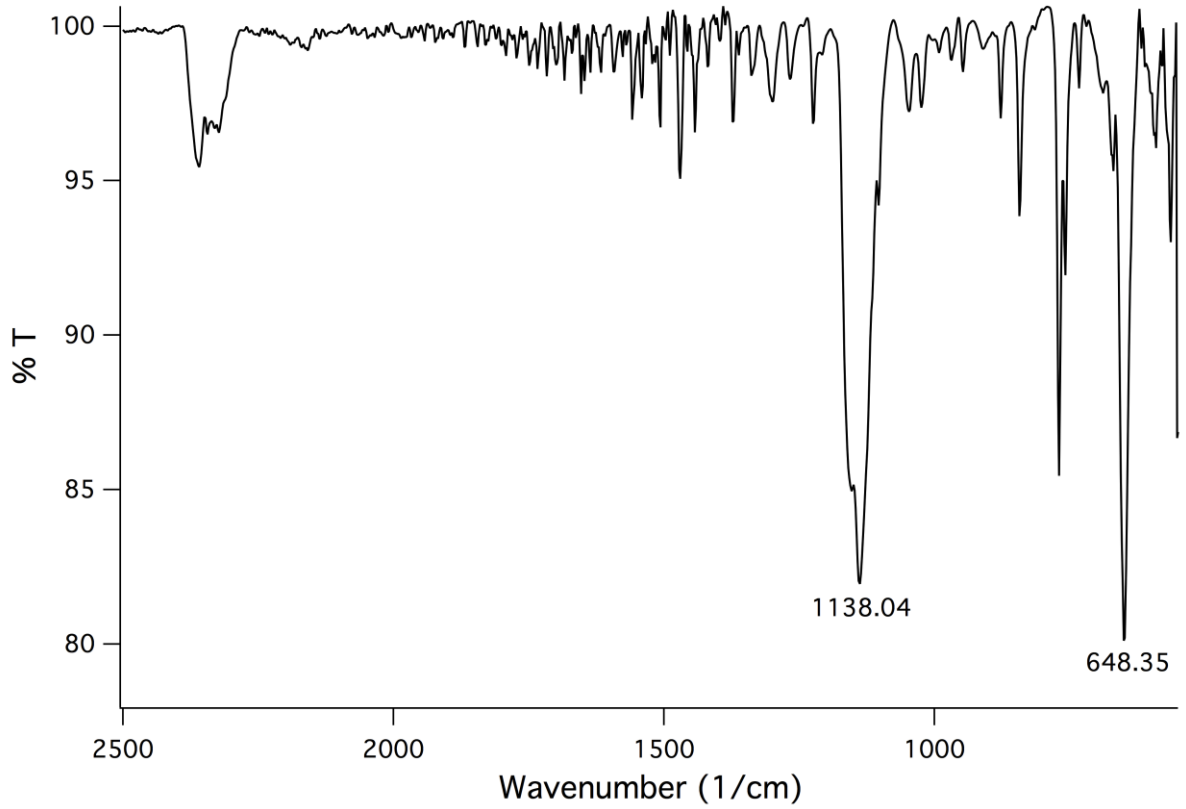

Figure S24. FT-IR spectra of $Ni_2(L^1)(CS_2)_2$ (**2**).

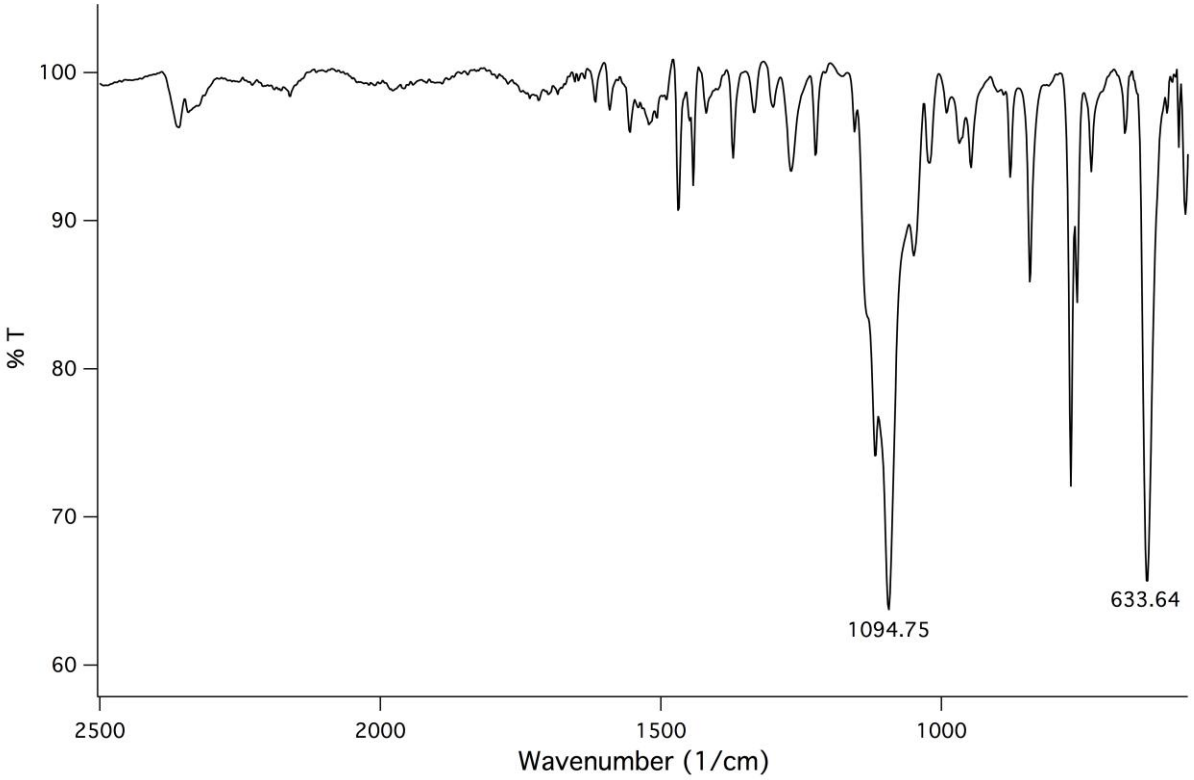

Figure S25. FT-IR spectra of $Ni_2(L^1)(^{13}CS_2)_2$ (**2**-$^{13}CS_2$).

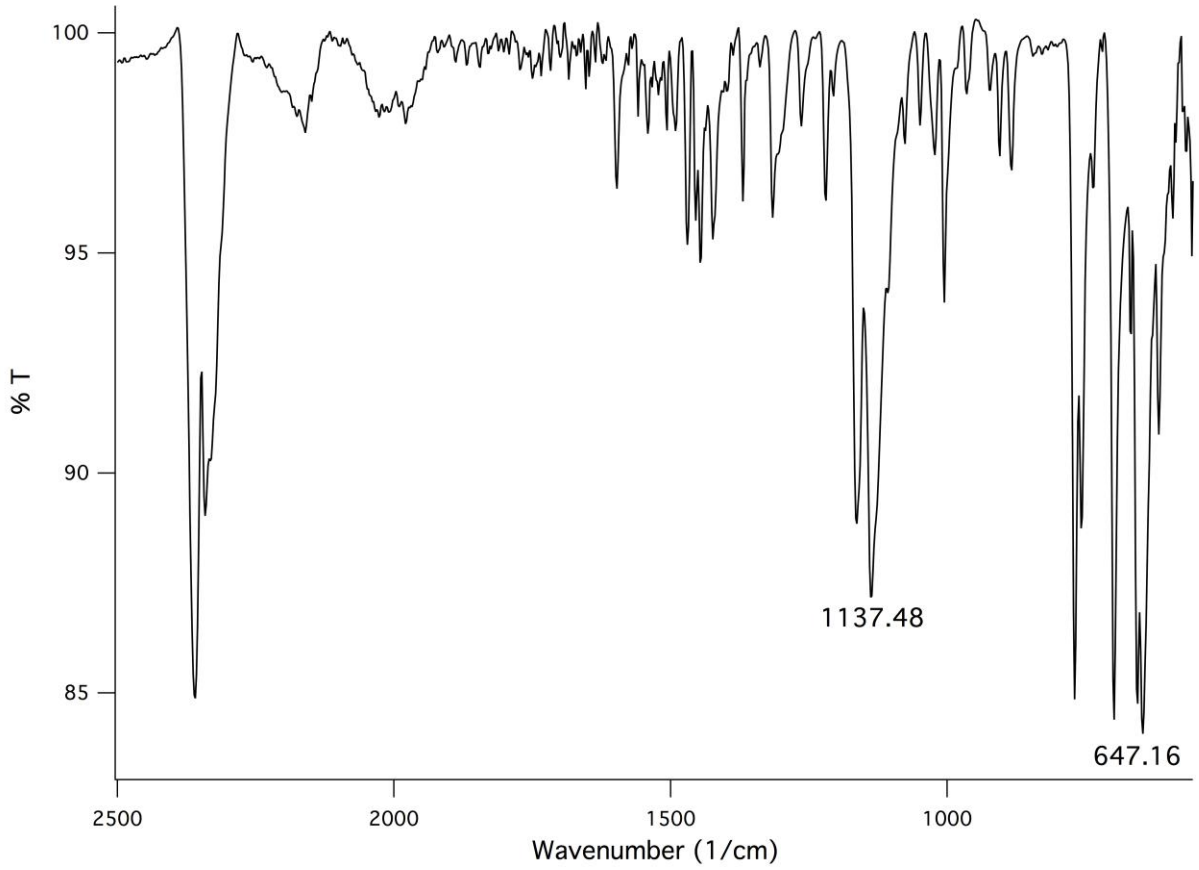

Figure S26. FT-IR spectra of Ni(L^2)(CS_2) (**4**).

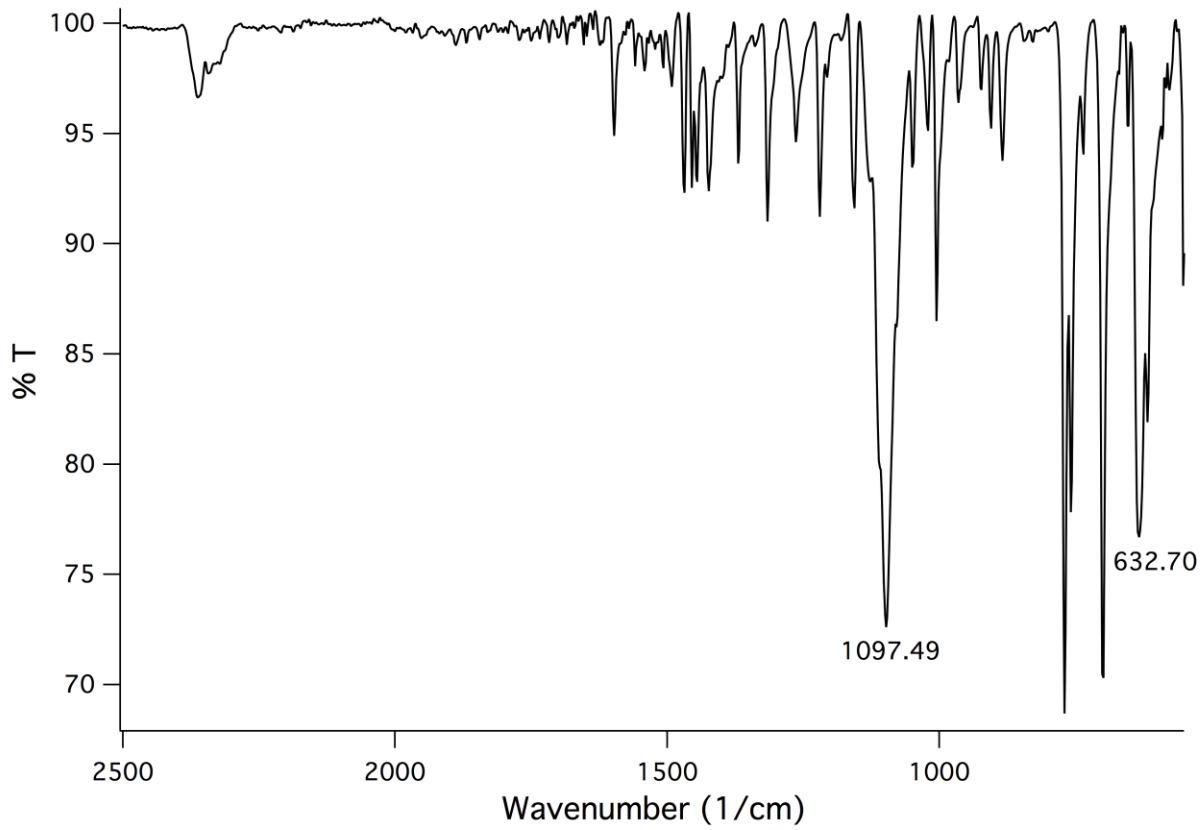

Figure S27. FT-IR spectra of Ni(L^2)($^{13}CS_2$) (**4**-$^{13}CS_2$).

8. Computational Details. Electronic structure calculations were carried out using density functional theory (DFT) [3] as implemented in Gaussian09. [4] Geometry optimizations were performed at the BP86/LANL2DZ/6-31G(d,p)[56789] level of theory with no symmetry constraints. We chose to use a pure functional here, BP86 compared to B3LYP in our previous report,[1] to allow for the use of density fitting[10] which significantly sped up geometry optimizations for the dinickel complex. All optimized structures were confirmed to have stable wavefunctions,[11,12] and to be local minima by analyzing the harmonic frequencies. [13] Cartesian coordinates and frequencies for the two species can be found in Tables S1 and S2, respectively.

As Figure S27 shows, the electronic structure of the dinickel complex **2** is the same as for the mononickel complex **4**. The HOMO (138/139) is a linear combination of the metal-d and sulfur-p orbitals, and the LUMO (140/141) is the π^* orbital of iminopyridine, with the exception that you get linear combinations between both Ni/iminopyridine fragments unlike in complex **4**. We have plotted the in- and out-of-phase orbitals side-by-side in the MO plot to emphasize their near degeneracy, showing weak electronic coupling across the bridge between the Ni/iminopyridine fragments. We show only the lowest energy minimum structure here.

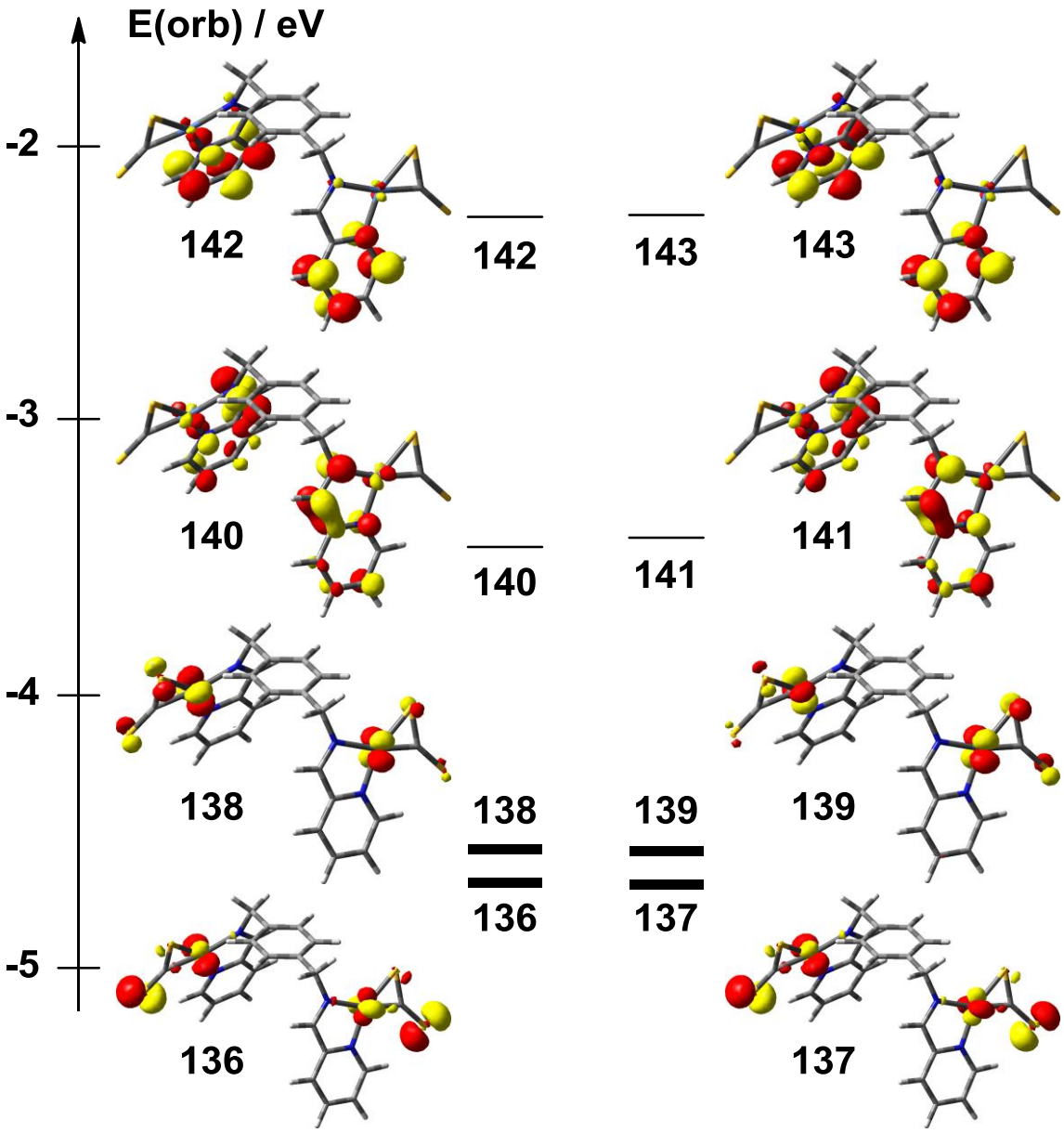

Figure S28. Frontier orbital diagram of **2**. Doubly occupied and unoccupied orbitals represented by bold and normal lines, respectively. All orbitals are plotted using an isosurface value of 0.05 both here and in Figure 4 of the main text.

Table S1. Cartesian coordinates (Å) for optimized structures of **2** and **4**.

2

C	2.079558	-1.899228	1.010234
C	3.214499	-2.655487	1.336174
C	3.235347	-3.467749	2.486777
C	2.095032	-3.507184	3.312884
C	0.962335	-2.746111	2.990283
C	0.940044	-1.936938	1.837557
H	2.080355	-1.268459	0.113856
H	4.091108	-2.620885	0.677081
H	2.098644	-4.128496	4.215835
H	0.079512	-2.793943	3.640191
C	-0.292233	-1.101596	1.511133
H	-1.161988	-1.477628	2.085888
H	-0.531734	-1.166453	0.435479
C	4.483621	-4.269169	2.836704
H	4.212522	-5.289597	3.158933
H	5.139938	-4.346622	1.947054
N	5.213686	-3.647102	3.959340
N	-0.058297	0.325224	1.810806
C	-0.470292	0.806095	2.949396
H	-1.017183	0.199336	3.689905
C	6.221466	-2.863510	3.699118
H	6.575668	-2.668514	2.673391
C	6.879665	-2.231245	4.836394
C	7.972257	-1.355166	4.733487
N	6.327333	-2.574026	6.050207
C	8.518262	-0.807677	5.903247
H	8.379645	-1.111555	3.746249
C	6.860992	-2.043203	7.172673
C	7.950399	-1.160100	7.138923
H	9.369240	-0.120861	5.850898
H	6.383394	-2.358777	8.111683
H	8.343857	-0.758511	8.078076
C	-0.172507	2.207042	3.223326
C	-0.535545	2.878929	4.401732
N	0.510691	2.832241	2.204373
C	-0.189239	4.229657	4.549391
H	-1.079712	2.341183	5.185735
C	0.838840	4.134682	2.354266
C	0.508519	4.862424	3.507128
H	-0.458866	4.776421	5.458770
H	1.376702	4.581794	1.505606
H	0.798771	5.915465	3.577484
Ni	4.881457	-3.844789	5.914926
Ni	0.826807	1.701920	0.672670
C	1.638751	2.695877	-0.647412
C	4.322259	-4.297991	7.609521
S	3.370959	-5.284952	6.593947
S	1.410450	1.169785	-1.374981
S	4.625744	-3.910022	9.167932
S	2.223620	4.202272	-0.892289

4

C	1.024526	1.055386	0.601905
H	1.645975	1.702785	1.240918
N	1.326626	-0.189212	0.384885
Ni	0.014356	-1.077850	-0.827916
C	-0.596766	-2.787342	-1.531495
S	0.945000	-3.198985	-1.275995
S	-2.145352	-2.645395	-1.894355
C	-0.185911	1.594616	-0.022699
C	-2.006039	1.088763	-1.405059
C	-0.619966	2.918670	0.134589
C	-2.497864	2.400847	-1.294827
H	-2.525430	0.331605	-2.000553
C	-1.797265	3.329078	-0.513052
H	-0.042408	3.611896	0.754665
H	-3.418290	2.676394	-1.817762
H	-2.158330	4.356718	-0.406729
N	-0.876859	0.688365	-0.785685
C	3.518681	-1.278439	-0.045719
C	4.050939	-2.579086	0.069628
C	3.932442	-0.454893	-1.113335
C	4.985065	-3.048939	-0.867998
H	3.744926	-3.221362	0.904937
C	4.860890	-0.928018	-2.053042
H	3.533195	0.561956	-1.212034
C	5.387142	-2.225761	-1.933045
H	5.399096	-4.057592	-0.764495
H	5.176998	-0.281404	-2.878622
H	6.112952	-2.593009	-2.666282
C	2.536417	-0.767908	0.997751
H	2.203611	-1.604933	1.638674
H	3.007518	-0.009736	1.656648

Table S2. Frequencies (cm^{-1}) for optimized structures of **2** and **4**.

2

5.1818	11.9155	12.4081
25.9637	26.6556	36.9066
45.3892	54.8766	59.2170
60.0255	77.6280	92.7126
98.3389	111.7321	127.2855
127.7716	155.2031	174.7145
174.8754	188.4181	191.6533
228.4361	242.1085	269.8143
277.7304	293.6624	307.6754
308.9239	312.1262	330.1953
348.8200	355.5316	363.9434
367.1051	400.3866	403.7404
411.3661	421.5640	423.3688
427.9403	455.2550	457.9297
473.9424	492.0548	492.4085
504.7788	514.2114	520.9041
610.5333	634.1567	637.3380
638.3144	643.7527	643.7745
655.8236	662.5277	702.9926
722.1339	724.2204	744.1798
747.9226	781.1334	804.4322
818.2315	835.6307	865.3261
867.0452	867.1428	868.7022
898.2135	900.7688	925.1553
927.2631	944.2042	944.2514
958.4405	974.6004	975.2494
975.3583	1000.3720	1001.1900
1007.7484	1019.2987	1024.5848
1044.7606	1044.7737	1104.4263
1104.8343	1121.2447	1152.7525
1152.7916	1182.2697	1188.9984
1192.1443	1193.0355	1193.9841
1199.2168	1199.3883	1227.1934
1227.5679	1296.4968	1296.5291
1310.5919	1314.5011	1315.1572
1319.6482	1326.7039	1352.8617
1359.4416	1364.3430	1418.2498
1436.9158	1437.1119	1465.3038
1465.3784	1467.7285	1468.5605
1508.6621	1545.5157	1545.7144
1580.2787	1594.2350	1594.2864
1600.4680	1601.0226	1612.8951
2959.8434	2959.9573	3033.5090
3033.5600	3048.4385	3048.4656
3065.0456	3065.0844	3100.6275
3101.8771	3122.4694	3124.0297
3126.1146	3126.1272	3137.6811
3137.6956	3149.1066	3149.1210

4

15.2757	21.0504	40.2939
43.3892	45.8215	75.8520
77.1653	96.5592	138.3203
145.4224	179.8550	231.0544
250.4157	274.6245	279.5487
314.9956	324.7940	346.2419
399.0958	410.5144	422.7691
455.8114	461.5932	492.7254
502.5132	599.3664	603.9221
610.7956	641.1460	659.6500
686.4616	728.1388	734.0283
753.9188	804.1315	822.1314
866.8881	878.9081	891.5846
924.0423	934.3646	946.4630
951.1761	971.4029	985.2413
985.3932	1006.5128	1027.8364
1037.2416	1048.8183	1087.1316
1108.5099	1162.4339	1164.7494
1178.8592	1189.5865	1210.2229
1230.0613	1290.6947	1298.8190
1320.7336	1332.5066	1358.5873
1364.2839	1394.0642	1439.0335
1445.5641	1453.3364	1470.1977
1493.9002	1563.7055	1588.2678
1594.5076	1602.8769	1618.0949
2951.1361	3019.4322	3068.1530
3105.5199	3106.2340	3128.8249
3136.7713	3142.0041	3146.2068
3147.3439	3155.0263	3165.0196

9. Electrochemistry

The electrochemical properties were determined by CV on a BAS Epsilon system. Samples were prepared in anhydrous *N,N'*-Dimethylformamide with tetrabutylammonium hexafluorophosphate (0.1 M) as the supporting electrolyte. The redox potentials were found versus an Ag/Ag^+ reference electrode. The Fc/Fc^+ potential was determined vs. the Ag/Ag^+ electrode using average based on 10 observations.

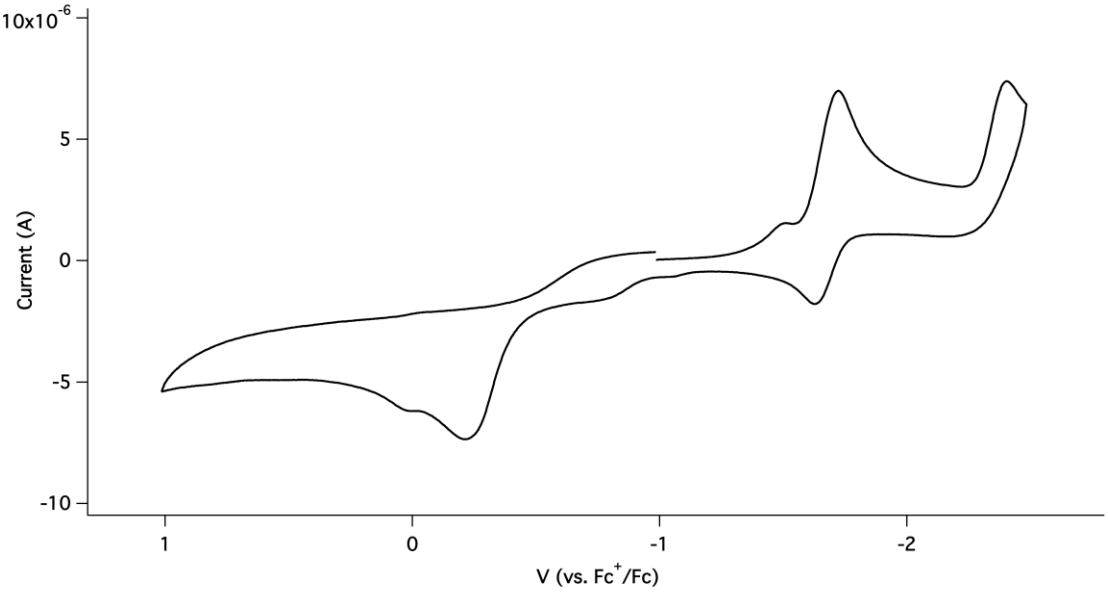

Figure S29. Cyclic voltammogram of $Ni_2Lig^1(CS_2)_2$ (0.1 M $[N(n\text{-}Bu)_4](PF_6)$ in DMF, 25 ^0C, Platinum working electrode, 100 mV/s scan rate).

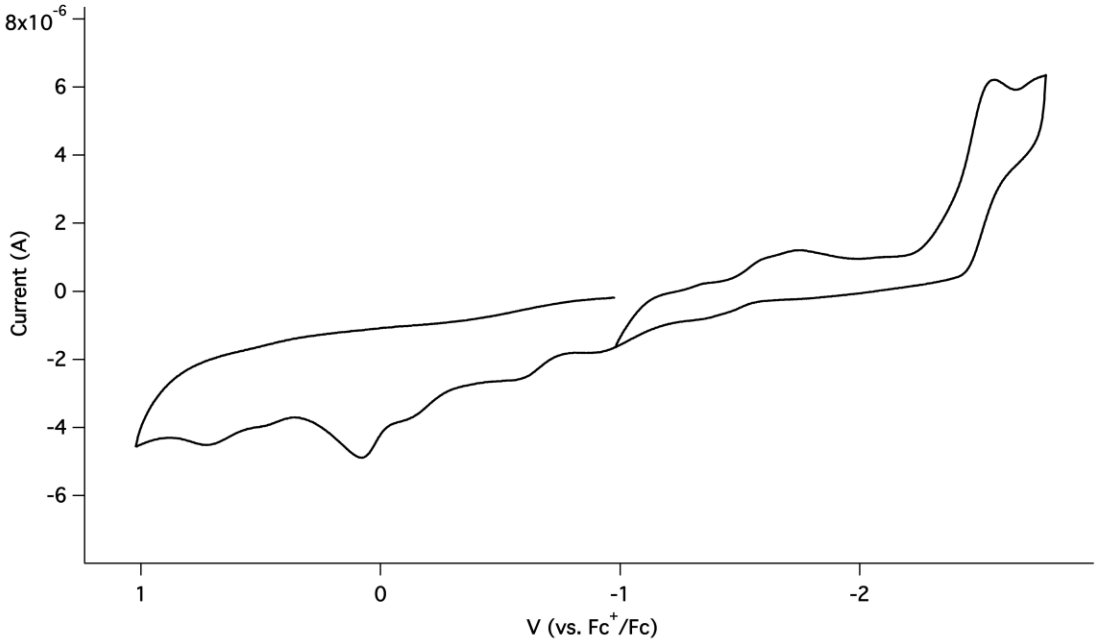

Figure S30. Cyclic voltammogram of $Ni_2Lig^1(COD)_2$ (0.1 M $[N(n\text{-}Bu)_4](PF_6)$ in DMF, 25 ^{0}C, Platinum working electrode, 100 mV/s scan rate).

10. References

[1]. Bheemaraju, A.; Lord, R.L.; Müller, P.; Groysman, S. *Organometallics* **2012**, *31*, 2120.
[2]. Volpe, E. C.; Wolczanski, P. T.; and Lobkovski, E. B. *Organometallics*, **2010**, *29*, 364.
[3]. Parr, R. G.; Yang, W. *Density-functional theory of atoms and molecules*; Oxford University Press: New York, 1989.
[4]. Frisch, M. J.; Trucks, G. W.; Schlegel, H. B.; Scuseria, G. E.; Robb, M. A.; Cheeseman, J. R.; Scalmani, G.; Barone, V.; Mennucci, B.; Nakatsuji, G. A. P. H.; Caricato, M.; Li, X.; Hratchian, H. P.; Izmaylov, A. F.; Bloino, J.; Zheng, G.; Sonnenberg, J. L.; Hada, M.; Ehara, M.; Toyota, K.; Fukuda, R.; Hasegawa, J.; Ishida, M.; Nakajima, T.; Honda, Y.; Kitao, O.; Nakai, H.; Vreven, T.; J. A. Montgomery, J.; Peralta, J. E.; Ogliaro, F.; Bearpark, M.; Heyd, J. J.; Brothers, E.; Kudin, K. N.; Staroverov, V. N.; Keith, T.; Kobayashi, R.; Normand, J.; Raghavachari, K.; Rendell, A.; Burant, J. C.; Iyengar, S. S.; Tomasi, J.; Cossi, M.; Rega, N.; Millam, J. M.; Klene, M.; Knox, J. E.; Cross, J. B.; Bakken, V.; Adamo, C.; Jaramillo, J.; Gomperts, R.; Stratmann, R. E.; Yazyev, O.; Austin, A. J.; Cammi, R.; Pomelli, C.; Ochterski, J. W.; Martin, R. L.; Morokuma, K.; Zakrzewski, V. G.; Voth, G. A.; Salvador, P.; Dannenberg, J. J.; Dapprich, S.; Parandekar, P. V.; Mayhall, N. J.; Daniels, A. D.; Farkas, O.; Foresman, J. B.; Ortiz, J. V.; Cioslowski, J.; Fox, D. J. *Gaussian 09, Revision C.01* Wallingford CT, 2010.
[5]. Becke, A. D. *Phys. Rev. A* **1988**, *38*, 3761.
[6]. Perdew, J.P. *Phys. Rev. B* **1986**, *33*, 8822.
[7]. Hay, P.J.; Wadt, W.R. *J. Chem. Phys.* **1985**, *82*, 270.
[8]. Wadt, W.R.; Hay, P.J. *J. Chem. Phys.* **1985**, *82*, 284.
[9]. Hay, P.J.; Wadt, W.R. *J. Chem. Phys.* **1985**, *82*, 299.
[10]. Dunlap, B.I. *J. Mol. Struct. (Theochem)* **2000**, *529*, 37.
[11]. Schlegel, H. B.; McDouall, J. J. In *Computational Advances in Organic Chemistry*; Ögretir, C., Csizmadia, I. G., Eds.; Kluwer Academic: Amsterdam, The Netherlands, 1991.
[12]. Bauernschmitt, R.; Ahlrichs, R. *J. Chem. Phys.* **1996**, *104*, 9047.
[13]. Schlegel, H. B. *J. Comput. Chem.* **1982**, *3*, 214.